

1 Phase-equilibrium geobarometers for silicic rocks based on rhyolite-MELTS. Part 5: Principles
2 for multiple-phase geobarometry with examples from plagioclase + orthopyroxene ± quartz ±
3 magnetite assemblages

4

5 Sarah L. Smithies

6 Corresponding author

7 School of Earth and Environment, University of Canterbury, Christchurch, New Zealand

8 <https://orcid.org/0000-0002-7734-2952>

9 sarah.smithies@canterbury.ac.nz

10

11 Guilherme A. R. Gualda

12 Department of Earth and Environmental Sciences, Vanderbilt University, TN, USA

13 <https://orcid.org/0000-0003-0720-2679>

14

15 Lydia J. Harmon

16 Department of Geology, Occidental College, CA, USA

17 <https://orcid.org/0000-0002-9985-705X>

18

19

20 Keywords:

21 Geobarometry, rhyolite-MELTS, phase equilibrium, thermodynamics, Taupō Volcanic Zone,
22 Puyehue-Cordón Caulle

23 Abstract

24 The quartz + feldspar rhyolite-MELTS phase-equilibrium geobarometer is a useful tool for
25 calculating equilibration pressures of rhyolitic magmas. However, it is limited by requiring
26 quartz saturation in magma. Here, we employ the principles from Parts 1-4 to move beyond
27 modeling a specific mineral assemblage. We demonstrate methods for carefully interpreting
28 the rhyolite-MELTS geobarometry results to constrain equilibration pressure in quartz-
29 undersaturated dacites to rhyolites, and where quartz saturation is uncertain. We show
30 examples of storage pressure calculations from quartz-absent rhyodacites to rhyolites from
31 Puyehue-Cordón Caulle (PCC), Chile; and examples of equilibration between extracted
32 rhyolitic melt compositions and unknown mush mineral assemblages from the Taupō Volcanic
33 Zone, New Zealand. In this case, orthopyroxene + plagioclase pressures can be used. However,
34 orthopyroxene saturation pressure results are higher at lower modelled oxygen fugacity. This
35 can be resolved by modelling at independently constrained f_{O_2} , or by modelling at a range of
36 f_{O_2} to search for orthopyroxene + magnetite + feldspar co-saturation. We show that
37 orthopyroxene + magnetite + feldspar pressures for PCC are consistent with results from other
38 geobarometers and occur within error of the f_{O_2} calculated from Fe-Ti oxides. If quartz
39 saturation is uncertain, quartz + feldspar pressures are a maximum and pyroxene-bearing
40 pressures at low f_{O_2} are a minimum. For uncertain mineral assemblages, the coincidence of
41 multiple phases (≥ 3) saturating together at reasonable f_{O_2} could be used to infer the
42 equilibrium mineral assemblage. Careful inspection of rhyolite-MELTS geobarometry results
43 therefore gives nuanced information about equilibration pressure, mineral assemblage, and
44 f_{O_2} .

45 Introduction

46 A fundamental problem in igneous petrology is constraining the pressure of magma storage
47 before eruption. Pressure has critical implications for understanding the processes that drive
48 eruption (Caricchi, et al. 2021; Gonnermann and Manga 2007). Pressures can be converted to
49 depth assuming lithostatic conditions to estimate the depth and geometry of magma bodies
50 (Black and Andrews 2020; Cooper, et al. 2012), and therefore the pre-eruptive architecture of
51 magma systems (Edmonds, et al. 2019; Gualda, et al. 2018; Wieser, et al. 2023). These magma

52 system models are useful in combination with geophysical datasets to interpret the unrest
53 signals of modern volcanos (Giordano and Caricchi 2022; Magee, et al. 2018; Pritchard, et al.
54 2018).

55 There are many geobarometers to estimate magma pressure from compositional parameters
56 such as mineral compositions (e.g., Hammarstrom and Zen 1986; Jorgenson, et al. 2022;
57 Mutch, et al. 2016; Putirka 2008; Ridolfi, et al. 2010), volatile contents (e.g., Anderson Jr, et al.
58 1989; Burnham 1994; Liu, et al. 2005; Newman and Lowenstern 2002; Papale, et al. 2006;
59 Wallace, et al. 1995), and melt compositions (e.g., Blundy 2022; Blundy and Cashman 2001;
60 Gualda and Ghiorso 2013b; Gualda and Ghiorso 2014; Herzberg 2004; Voigt, et al. 2017;
61 Weber and Blundy 2024; Wilke, et al. 2017; Yang, et al. 1996). Melt-only geobarometers
62 search for the pressure that melt of a known composition equilibrated with mineral phases of
63 interest. A distinct advantage of melt-only geobarometers is that major-element melt
64 compositions are relatively easy to obtain (by X-ray fluorescence spectroscopy (XRF),
65 wavelength dispersive X-ray spectroscopy (WDS) attached to an electron microprobe (EMP),
66 or energy dispersive X-ray spectroscopy (EDS) attached to a scanning electron microprobe
67 (SEM)) compared to other common geobarometry techniques (e.g., measuring H₂O-CO₂ in
68 melt inclusions by fourier transform infrared spectroscopy or secondary ion mass
69 spectrometry; measuring mineral rim and core compositions by WDS-EMP). Unlike
70 geobarometers that use the composition of multiple phases (e.g., amphibole-plagioclase
71 Holland and Blundy 1994; Molina, et al. 2021; orthopyroxene-clinopyroxene, Putirka 2008),
72 melt-only geobarometers do not require the assumption of equilibrium between paired phase
73 compositions. Melt-only geobarometers can either be derived from empirical relationships
74 extrapolated from experimental datasets (Blundy 2022; Blundy and Cashman 2001; Herzberg
75 2004; Voigt, et al. 2017; Weber and Blundy 2024; Wilke, et al. 2017; Yang, et al. 1996), or from
76 phase-equilibria models (Bégué, et al. 2014b; Gualda and Ghiorso 2014; Harmon, et al. 2018;
77 Pamukçu, et al. 2015). We focus on phase-equilibrium geobarometers, which have the
78 advantage of being grounded in thermodynamic theory and better suited to interpolation and
79 extrapolation to unknown compositions.

80 In the last decade, there have been rapid advancements in using phase-equilibria to find the
81 equilibration pressure of rhyolitic magma (Bégué, et al. 2014b; Gualda and Ghiorso 2014;
82 Harmon, et al. 2018; Pamukçu, et al. 2015). Gualda and Ghiorso (2014) introduced a

83 geobarometer that searches for the equilibration pressure between melt, quartz, and one or
84 two feldspars (hereafter referred to as the “quartz + feldspar geobarometer”). They estimate
85 pre-eruptive crystallization pressures using as input the composition of quartz-hosted melt
86 (glass) inclusions in pyroclastic rocks from the Bishop Tuff, under the assumption that the glass
87 compositions represent melt that equilibrated with quartz and one or more feldspars under
88 pre-eruptive storage conditions (Figure 1). Subsequent work used matrix glass compositions
89 to represent pre-eruptive melt (e.g., Pamukçu, et al. 2015 and others). The Gualda and
90 Ghiorso (2014) quartz + feldspar geobarometer uses the rhyolite-MELTS version 1.0 model to
91 calculate the equilibration pressure of quartz, feldspar, and melt. The quartz + feldspar
92 geobarometer has been applied to many silicic systems, including the Taupō Volcanic Zone
93 (Bégué, et al. 2014b; Gualda, et al. 2018; Gualda, et al. 2019b; Harmon, et al. 2024a; Harmon,
94 et al. 2024b; Pamukçu, et al. 2021; Pamukçu, et al. 2020; Smithies, et al. 2024; Smithies, et al.
95 2023), Peach Spring Tuff, Silver Creek Caldera (Foley, et al. 2020; Pamukçu, et al. 2015), Bishop
96 Tuff, Long Valley Caldera (Gualda and Ghiorso 2013a; Gualda, et al. 2022), the Youngest Toba
97 Tuff, northern Sumatra (Pearce, et al. 2020); and Hokkaido, Japan (Pitcher, et al. 2021).
98 Generally, rhyolite-MELTS quartz + feldspar geobarometry results compare well to
99 independent volatile and amphibole geobarometry estimates on the same systems (Bégué, et
100 al. 2014b; Gualda, et al. 2019a; Pamukçu, et al. 2015; Pamukçu, et al. 2021). Errors on quartz
101 + feldspar geobarometry results calculated from XRF and EDS-SEM compositions are on the
102 order of 10-20 MPa 1σ (Gualda, et al. in review; Pamukçu, et al. 2021; Pitcher, et al. 2021;
103 Smithies, et al. 2024; Smithies, et al. 2023). These errors are equivalent to 0.4-0.8 km depth
104 assuming a crustal density of 2.7 g cm^{-3} , making the quartz + feldspar geobarometer a useful
105 and relatively precise estimate of pressure and depth.

106 Although the rhyolite-MELTS quartz + feldspar geobarometer is useful in many rhyolitic
107 systems, it is limited to magma that is saturated in quartz. This limits its usefulness to rhyolitic
108 compositions, and to magma where we know the equilibrium mineral assemblage with
109 confidence. This is a potential problem, as the mineral assemblage in volcanic rocks is often a
110 complex mixture of crystals grown in equilibrium with the surrounding melt/glass
111 (“autocrysts”), and crystals incorporated from other parts of the magmatic system or from the
112 country rock (“antecrysts” and “xenocrysts”) (e.g., Bachmann, et al. 2002). The rock mineral
113 assemblage is therefore not unequivocal proof of the equilibrium mineral assemblage.

114 Uncertainty over whether or not quartz is saturated is also a significant limitation of using
115 rhyolite-MELTS geobarometry to calculate the pressure that melt was extracted from the
116 mush (hereafter “extraction pressure”, Gualda, et al. 2019b). This method assumes that the
117 bulk composition of erupted magma represents the composition of the melt that equilibrated
118 with the mush (Figure 1; Blundy 2022; Gualda, et al. 2019b). In this scenario, quartz saturation
119 is uncertain as we must infer the mineral assemblage of the mush from erupted mush
120 fragments or from the composition of the erupted magma. This leaves us with the question:
121 how can phase-equilibria models be used to constrain pressure for systems where we are
122 uncertain if quartz is saturated?

123 Harmon, et al. (2018) introduced a geobarometer that uses the same rhyolite-MELTS
124 thermodynamic model as Gualda and Ghiorso (2014) but searches for the pressure of
125 equilibration between feldspar (typically plagioclase) and one or two pyroxenes (hereafter the
126 “plagioclase + pyroxene geobarometer”). Harmon, et al. (2018) tested the plagioclase +
127 pyroxene geobarometer on basaltic-andesite compositions and found that it could find
128 reasonable pressure estimates. Other studies subsequently applied the plagioclase + pyroxene
129 geobarometer to dacitic to rhyolitic systems (Foley, et al. 2020; Gualda, et al. 2019b; Harmon,
130 et al. 2024b; Pamukçu, et al. 2021; Smithies, et al. 2024; Smithies, et al. 2023). The plagioclase
131 + pyroxene geobarometer is sensitive to oxygen fugacity (f_{O_2}) due to the strong partitioning of
132 Fe^{2+} relative to Fe^{3+} in pyroxene. Although independently estimated f_{O_2} (e.g. from Fe-Ti oxides)
133 can be used as an input into the geobarometry calculation, there is some uncertainty over
134 whether the f_{O_2} estimated from Fe-Ti oxides records pre-eruptive conditions, or whether it
135 may have re-equilibrated during syn-eruptive conditions (Pitcher, et al. 2021; Tomiya, et al.
136 2013). This makes constraining pressure with the plagioclase + pyroxene geobarometer
137 challenging.

138 The goal of this study is to demonstrate the efficacy of rhyolite-MELTS across a range of
139 different observed and inferred mineral assemblages. By combining our understanding of
140 plagioclase + pyroxene phase-equilibria geobarometry (Harmon, et al. 2018) with our
141 understanding of quartz + feldspar phase-equilibria geobarometry (Gualda and Ghiorso 2014)
142 to better constrain pressure in quartz-undersaturated dacites and rhyolites, we demonstrate
143 that the principles established in this series (Bégué, et al. 2014b; Gualda and Ghiorso 2014;
144 Harmon, et al. 2018; Pamukçu, et al. 2015) can be adapted to a wider range of igneous

145 systems. We explore examples from two systems: extraction of rhyolitic magma from an
146 unknown mush mineral assemblage in the Taupō Volcanic Zone (TVZ), Aotearoa New Zealand;
147 and pre-eruptive magma storage of quartz-absent rhyodacites to rhyolites from Puyehue-
148 Cordón Caulle (PCC), Chile. Using these case studies, we demonstrate that rhyolite-MELTS
149 geobarometry results can be interpreted to give a more nuanced understanding of melt-only
150 pressures in the presence or absence of quartz.

151 **Methods**

152 **Modelling approach for determining pressure and equilibrium mineral assemblage**

153 In Figure 2 we show an example of a quartz + feldspar geobarometry result following the
154 method of Gualda and Ghiorso (2014). The calculations were performed on a pressure-
155 temperature grid, calculating the equilibrium assemblage at 1°C temperature steps and 25
156 MPa pressure steps. The melt composition that we are interested in (in Figure 2, a whole-rock
157 composition for extraction pressure) was input as the bulk composition of the system. The
158 saturation surfaces represent the highest temperature that each mineral phase is present for
159 a given pressure. The saturation surfaces were interpolated between each 25 MPa interval.

160 At high temperatures, the simulated magma is liquid (i.e. above the liquidus) with an exsolved
161 fluid phase. Therefore, above the liquidus, the melt composition is the same as the bulk
162 composition of the system. At temperatures below the liquidus, the system has liquid, solids
163 and an exsolved fluid phase. This means that below the liquidus, crystallization of solid phases
164 changes the composition of the melt, such that the simulated melt does not have the same
165 composition as the bulk composition. This is an important realisation, as only the region at or
166 above the liquidus has melt with the same composition as the bulk composition of the system,
167 which is the measured composition input by the user (either a whole-rock or glass
168 composition). Therefore, only pressures and temperatures in the region at or above the
169 liquidus are acceptable for the measured melt composition, while the region below the
170 liquidus does not yield acceptable pressure or temperature solutions for the measured melt
171 composition. If we are searching for an equilibrium assemblage of melt (represented by the
172 measured composition) and minerals, the only part of the diagram in Figure 2 where this is
173 possible is the liquidus. In the example in Figure 2, if we assume that both orthopyroxene and

174 plagioclase are in equilibrium with the input melt composition, there is only one possible
175 pressure and temperature, at 106 MPa and 800 °C. The intersection of the orthopyroxene and
176 plagioclase saturation surfaces therefore gives us the pressure of equilibration between
177 orthopyroxene, plagioclase, and the melt.

178 The saturation surfaces are interpolated between the 25 MPa pressure intervals. To calculate
179 the saturation surface intersections, we use the parabola-fitting procedure described by
180 Gualda and Ghiorso (2014). The residual temperature between the saturation surfaces at each
181 25 MPa interval is calculated, then a parabola is fitted to the minimum residual and two points
182 on either side of the minimum (Figure 2). This parabola-fitting procedure is only applied if the
183 minimum is ≤ 5 °C (the minimum temperature threshold in Figure 2). Gualda and Ghiorso
184 (2014) show that the minimum of the parabola is a satisfactory estimate of the saturation
185 surface intersection. When the minimum of the residual curve is never ≤ 5 °C over the pressure
186 range investigated, we conclude that the rhyolite-MELTS geobarometer finds no satisfactory
187 pressure for the melt composition and mineral assemblage of interest.

188 **Case study geobarometry calculations**

189 In this study we show examples from two case studies: rhyolites of the Taupō Volcanic Zone
190 (TVZ), Aotearoa New Zealand; and rhyodacites to rhyolites from Puyehue-Cordón Caulle (PCC),
191 Chile. From the TVZ we show examples of extraction pressure calculations, using whole-rock
192 compositions to model the pressure the eruptible magma was extracted from a mush with
193 unknown mineral assemblage (Figure 1). The TVZ was selected as an example of a system
194 where the erupted magma is quartz-bearing but we are uncertain of the mineralogy of the
195 mush (Table 1). From PCC we show examples of pre-eruptive storage pressure calculations,
196 using glass compositions to model the pressure the melt was in equilibrium with the
197 phenocryst assemblage immediately prior to eruption. In contrast to the TVZ, PCC rhyolites
198 do not have quartz in either the phenocryst mineral assemblage (Table 1) or in the co-erupted
199 mush fragments (Winslow, et al. 2022).

200 In the TVZ we focus on five large (>50 km³ dense rock equivalent), caldera-forming eruptions
201 (Table 1). Previously published whole-rock compositions were collated from Smithies, et al.
202 (2023). Each sample (n=53) is an individual pumice clast collected from unwelded ignimbrite
203 deposits. Whole-rock compositions were collected by either XRF (Chimp, Pokai, Kaingaroa,

204 and Mamaku samples) or by inductively coupled plasma optical emission spectrometry
205 (Ohakuri samples). The pumice clasts have sparse (<8% by vol.) plagioclase + orthopyroxene +
206 Fe-Ti oxides ± quartz ± hornblende ± clinopyroxene phenocrysts (Table 1). All the samples are
207 rhyolitic in composition (Figure 3).

208 For each TVZ composition, we collated geobarometry calculations from Smithies, et al. (2023)
209 and performed additional calculations with the same methodology to expand the range of f_{O_2}
210 values. Geobarometry calculations were performed with the rhyolite-MELTS v.1.0 model with
211 an updated version of the MELTS_Excel interface (Gualda and Ghiorso 2015). The latest
212 version of MELTS_Excel and supporting documentation is distributed for free from
213 <http://melts.ofm-research.org>. Whole-rock compositions were input as the melt
214 composition. Equilibration calculations were performed in a pressure-temperature grid from
215 500 to 25 MPa in 25 MPa steps and from 1100 °C to 700 °C in 1 °C steps. We forced fluid
216 saturation at all pressures by setting H₂O to 15 wt.%; even though these are unrealistic H₂O
217 contents for most crustal magmas, the presence of exsolved water does not affect the
218 pressure calculations, and it guarantees that the melt is saturated in H₂O (see Ghiorso and
219 Gualda 2015; Gualda and Ghiorso 2014 for full discussion). The calculations were repeated
220 from 0.5 log units below the quartz-fayalite-magnetite (QFM) f_{O_2} buffer to 2 log units above
221 it in 0.5 log unit steps (QFM -0.5; QFM; QFM +0.5; QFM +1.0; QFM +1.5; QFM +2.0). For a
222 small subset of samples (POK_105A, POK_112A_A, OHK302B4) we repeated the calculations
223 at QFM -1.0, QFM -1.5, and QFM -2.0.

224 We include compositions from the three most recent large eruptions at PCC (Table 1). These
225 are relatively small (0.25-1.5 km³) eruptions, which generated both lava flows and pyroclastic
226 deposits (Lara, et al. 2006; Pistolesi, et al. 2015; Singer, et al. 2008). Compositions were
227 collated from Castro, et al. (2013); Schipper, et al. (2019); Seropian, et al. (2021). The samples
228 (n=33) are individual pyroclastic clasts. Each sample composition is a mean of 9-40 spot
229 compositions measured by WDS-EMP on fresh, unaltered glass. Phenocrysts are sparse in the
230 pyroclastic material (<15 vol.%) with an assemblage of plagioclase + orthopyroxene +
231 clinopyroxene + Fe-Ti oxides (Table 1). The bulk rock and glass compositions are rhyodacitic to
232 rhyolitic (Figure 3).

233 For each PCC composition, we collated geobarometry calculations from Seropian, et al. (2021)
234 and performed additional calculations with the same methodology to expand the range of f_{O_2}
235 values. The input parameters are the same as for the TVZ samples, except that glass
236 compositions were used to result in pre-eruptive storage pressure estimates (Figure 1), and
237 therefore the pressure-temperature grid was reduced to 400 to 25 MPa in 25 MPa steps and
238 from 1100 °C to 700 °C in 1 °C steps. We set H₂O to 10 wt.% to force fluid saturation (see
239 above). The calculations were repeated from 1 log unit below the nickel-nickel oxide (NNO)
240 f_{O_2} buffer to 1.5 log units above in 0.25 or 0.5 log unit steps (NNO -1.0; NNO -0.75; NNO -0.5;
241 NNO -0.25; NNO; NNO +0.5; NNO +1.0; NNO +1.5). For three samples (D60_17, A-gr12, B-gr2)
242 we ran additional calculations at NNO -1.5, NNO -2.0, and NNO -2.5. This is approximately
243 equivalent to the f_{O_2} range used for the TVZ samples.

244 Results

245 Geobarometry results

246 At the lowest f_{O_2} tested (QFM-0.5), the extraction pressures for the TVZ range from 68-381
247 MPa with a mean of 214 MPa (Figure 4). The modelled mineral assemblages are a mixture of
248 orthopyroxene + plagioclase (n=40), quartz + plagioclase (n=5), and plagioclase +
249 orthopyroxene + quartz (n=8). At higher f_{O_2} , the mean pressure result is higher (e.g., 291 MPa
250 at QFM+0.5) and there are fewer plagioclase + orthopyroxene results (e.g., n=16 at QFM+0.5)
251 and plagioclase + orthopyroxene + quartz results (e.g., n=1 at QFM+0.5) relative to the number
252 of quartz + plagioclase results (e.g., n=36 at QFM+0.5). At the highest f_{O_2} tested (QFM+2), the
253 TVZ extraction pressures range from 122-468 MPa with a mean of 327 MPa. At high f_{O_2}
254 (QFM+2) the results are entirely quartz + plagioclase mineral assemblages (n=50).

255 The PCC results are dominated by a plagioclase + orthopyroxene mineral assemblage at all f_{O_2}
256 tested (Figure 4). Quartz-bearing mineral assemblages only occur in a minority of samples
257 (n=3) at the highest f_{O_2} we tested (NNO+1 and NNO+1.5). The pressure results are strongly
258 dependent on f_{O_2} . At the lowest f_{O_2} tested (NNO-1.0) the pressures are relatively low, ranging
259 from 25-123 MPa with a mean of 80 MPa. At progressively higher f_{O_2} , the pressures increase.
260 At the highest f_{O_2} tested (NNO+1.5), the pressures range from 285-361 MPa with a mean of

261 324 MPa. At high f_{O_2} , some calculations repeatedly crashed, failing to return a result (n=6 at
262 NNO+0.5, n=9 at NNO+1, n=24 at NNO+1.5).

263 **The effect of f_{O_2} on the plagioclase + orthopyroxene results**

264 The equilibrium mineral assemblage results (and therefore pressure results) are sensitive to
265 f_{O_2} (Figure 5). In Figure 5a-d we show geobarometry results for the same composition as Figure
266 2 but using different f_{O_2} values. The input parameters for each calculation are identical except
267 for f_{O_2} . The effect of varying f_{O_2} on the orthopyroxene saturation temperature is evident. At
268 low f_{O_2} (QFM -0.5), which results in lower Fe^{3+}/Fe^{total} in the melt, the orthopyroxene saturation
269 temperature is high (Figure 5a). In this example, quartz is never in equilibrium with the
270 measured melt composition. Therefore, the only acceptable pressure solution is plagioclase +
271 orthopyroxene at 102 MPa. At more oxidising f_{O_2} and higher melt Fe^{3+}/Fe^{total} (Figure 6) the
272 orthopyroxene saturates at lower temperatures. Because the orthopyroxene saturation
273 temperature is lower, the plagioclase + orthopyroxene intersection occurs at higher pressures.
274 This leads to a negative correlation between f_{O_2} and plagioclase + orthopyroxene pressures
275 (Figure 6). The relationship between f_{O_2} and pressure is not linear (Figure 6), given that the
276 Fe^{3+}/Fe^{total} ratio does not vary linearly with f_{O_2} . For strongly reducing f_{O_2} values (e.g., <<QFM
277 or <<NNO, Figure 6), the majority of the iron in the system is reduced to Fe^{2+} . At strongly
278 reducing f_{O_2} the pressure values therefore become less dependent on f_{O_2} (Figure 6). At more
279 oxidising f_{O_2} (e.g., QFM +0.5, Figure 5c), the saturation temperature of orthopyroxene
280 decreases, so the orthopyroxene saturation surface intersects with quartz and plagioclase on
281 the liquidus. This means that it is possible for orthopyroxene, plagioclase, and quartz to be in
282 equilibrium together with melt of the measured composition, resulting in a three-phase
283 orthopyroxene + quartz + plagioclase pressure at 177 MPa. At even higher f_{O_2} (QFM +1, Figure
284 5d), the orthopyroxene saturation temperature decreases further, such that the
285 orthopyroxene saturation surface is below the quartz and plagioclase saturation surfaces. At
286 this f_{O_2} , orthopyroxene cannot be in equilibrium with quartz, plagioclase, and the measured
287 melt composition. The only acceptable pressure result is therefore quartz + plagioclase at 187
288 MPa. Importantly, the quartz + plagioclase pressure is the same as the three-phase
289 orthopyroxene + quartz + plagioclase pressure, within the error of the parabola curve-fitting
290 procedure (see Figure 2). In the cases in which quartz is not present, the quartz + plagioclase
291 pressure represents a maximum pressure, given that only at pressures below that intersection

292 can the melt of given composition be in equilibrium with plagioclase and not quartz – this
293 result is independent of f_{O_2} .

294 Discussion

295 **Dealing with unknown f_{O_2}**

296 The strong dependence of orthopyroxene + plagioclase \pm quartz pressures on f_{O_2} (Figures 5 &
297 6) leads to a challenge: how do we constrain pressure for orthopyroxene-bearing dacites and
298 rhyolites? Here, we discuss strategies for constraining pressure in the following scenarios: 1)
299 we are confident that quartz is in equilibrium with the melt; 2) we are confident that quartz
300 is NOT in equilibrium with the melt (but plagioclase and orthopyroxene are); 3) we are unsure
301 if quartz is in equilibrium with the melt.

302 Scenario 1: quartz is in equilibrium with the melt

303 If we are confident that quartz is saturated, we can use the rhyolite-MELTS geobarometer to
304 calculate the pressure of equilibration between the melt, quartz, and feldspar. For example,
305 many of the Taupō Volcanic Zone rhyolites have plagioclase and quartz phenocrysts, which we
306 are reasonably confident were in equilibrium with the surrounding melt (now quenched as
307 glass) (Bégué, et al. 2014b; Gualda, et al. 2018; Smithies, et al. 2023). These quartz +
308 plagioclase pressures are completely independent of f_{O_2} – note that the quartz and plagioclase
309 saturation surfaces shown in Figure 5 do not change with varying f_{O_2} . Orthopyroxene is also a
310 phenocryst phase in these rhyolites, so we could adjust f_{O_2} to find a value that gives a quartz
311 + plagioclase + orthopyroxene intersection. Importantly, the pressure of a three-phase
312 intersection is the same as from the two-phase quartz + plagioclase intersection. The search
313 in f_{O_2} space therefore does not give us any further constraint on pressure, only on f_{O_2} . This
314 demonstrates that the quartz + feldspar geobarometer of Gualda and Ghiorso (2014) is
315 sufficient to determine pressure in quartz-saturated systems without modelling additional
316 phases. Nonetheless, quartz + plagioclase + orthopyroxene geobarometry could be used to
317 find an f_{O_2} that is internally consistent with the rhyolite-MELTS model.

318 Scenario 2: quartz is NOT in equilibrium with the melt

319 The rhyolites from the recent PCC eruptions have plagioclase and orthopyroxene phenocrysts,
320 but quartz is absent (Table 1). This means that only a plagioclase + orthopyroxene \pm

321 clinopyroxene pressure solution would be acceptable. As the pyroxenes are sensitive to f_{O_2} ,
322 this makes constraining pressure more challenging. A first order approach is to use an f_{O_2} value
323 for the system that has been independently determined. Conveniently, the commonly used
324 oxythermobarometer of Ghiorso and Evans (2008) is internally consistent with the MELTS
325 family of thermodynamic models, so f_{O_2} calculated with this oxythermobarometer are
326 preferable for finding pressures. For example, f_{O_2} for the 2011 PCC eruption is estimated to
327 be between NNO -0.9 and NNO -0.8 using the Ghiorso and Evans (2008) oxythermobarometer
328 (Castro, et al. 2013; Jay, et al. 2014; Mingo 2019). The rhyolite-MELTS pyroxene + plagioclase
329 pressure estimates at NNO -1.0 and NNO -0.75 for the 2011 PCC eruption (i.e., 25-146 MPa)
330 are in excellent agreement with independent geobarometry and geophysical estimates of
331 magma storage depths for the same eruption (50-140 MPa; Table 2) (Seropian, et al. 2021).

332 Even for eruptions where f_{O_2} has not been determined, there is a limited range of f_{O_2} that
333 could be considered reasonable. Global compilations of erupted magmas from subduction
334 systems show a limited range of f_{O_2} between QFM and QFM +2 (Cottrell, et al. 2021; Ghiorso
335 and Evans 2008; Ghiorso and Gualda 2013). The extremely reducing f_{O_2} shown in Figure 6 are
336 therefore generally implausible.

337 An important caveat to using f_{O_2} constrained by Fe-Ti oxides is that we cannot be certain that
338 the f_{O_2} recorded by the Fe-Ti oxides was the f_{O_2} of the system at the pressure recorded by the
339 melt. Both Fe and Ti in Fe-Ti oxides can re-equilibrate rapidly (days) (Tomiya, et al. 2013; Van
340 Orman and Crispin 2010), so they are likely to record the eruptive conditions and immediately
341 prior to eruption rather than the longer-term pre-eruptive storage (years). During magma
342 storage and ascent, f_{O_2} is affected by complex open-system processes such as degassing
343 (Burgisser and Scaillet 2007). If this is the case, the f_{O_2} recorded by Fe-Ti oxides is not the f_{O_2}
344 of pre-eruptive storage. Using Fe-Ti oxides to estimate f_{O_2} is particularly problematic for
345 extraction pressures, as we are considering the equilibration of the melt recorded by the bulk-
346 rock, whereas the Fe-Ti oxide phenocrysts likely equilibrated with the melt preserved as glass.
347 (Figure 1).

348 In the absence of any information about f_{O_2} , we make two crucial observations that can
349 constrain a range of possible pressures. The first observation is that the plagioclase +
350 orthopyroxene pressure must always be less than the quartz + plagioclase pressure, as

351 orthopyroxene must saturate at a higher temperature than quartz in quartz-undersaturated
352 magma. Therefore, we can always constrain a maximum pressure in quartz-undersaturated
353 magma by taking the quartz + plagioclase pressure as a maximum. The second observation is
354 that at strongly reducing f_{O_2} values (e.g., <QFM-1.5, <NNO-1), as Fe^{3+}/Fe^{total} approaches 0, the
355 orthopyroxene + plagioclase pressures approach a constant value (Figure 6). We can therefore
356 also constrain a minimum pressure by calculating the pressure at strongly reducing conditions.
357 These two observations give us a range of possible pressures.

358 Scenario 3: quartz may or may not be in equilibrium

359 There are several scenarios in which we are uncertain whether the system is quartz-saturated
360 or not. Here, we show extraction pressures, in which we use whole-rock compositions from
361 the TVZ to represent the theoretical melt that equilibrated with the mush mineral assemblage
362 (Figure 1; Blundy 2022; Gualda, et al. 2019b). We are uncertain what mineral assemblage the
363 melt was extracted from, as the mush typically does not erupt. Based on occasionally erupted
364 mush fragments (Brown, et al. 1998; Burt, et al. 1998; Graeter, et al. 2015) and the
365 composition of the erupted rhyolites we can reasonably assume the mush in the TVZ is either
366 granodioritic (plagioclase + quartz + orthopyroxene) or dioritic (plagioclase + orthopyroxene).
367 This leaves us uncertain whether magmas erupted from the TVZ were extracted from mush
368 that is or is not quartz-saturated.

369 In cases in which we are uncertain of whether quartz is saturated or not, the quartz +
370 plagioclase pressures are the maximum possible pressures (see Figure 5), with lower pressures
371 possible for a plagioclase + orthopyroxene (Pamukçu, et al. 2021). This is also seen in Figure
372 4, which demonstrates that quartz + plagioclase pressures constitute a maximum bound on
373 possible pressures. Figure 4 also shows that a range of orthopyroxene + plagioclase pressures
374 is possible, depending on f_{O_2} . If there is some information about f_{O_2} , then the best estimate of
375 f_{O_2} for the system can be used to find both the likely pressure and the likely equilibrium
376 mineral assemblage. The PCC storage pressure results are only quartz-saturated at
377 unreasonably high f_{O_2} (>NNO +1), more than one log unit higher than the estimated f_{O_2} for
378 PCC (Figure 6). We would thus conclude – based on rhyolite-MELTS geobarometry – that PCC
379 magmas are unlikely to be quartz-saturated. This is in agreement with observations of natural
380 rocks, given that PCC volcanic rocks are typically quartz-absent (Table 1). In contrast, the
381 rhyolite-MELTS models show that some of the TVZ melts extracted from the mush could have

382 equilibrated with quartz at reasonable f_{O_2} (Figure 6). This agrees with evidence from mush
383 fragments co-erupted with TVZ rhyolites, some of which are quartz-bearing (Brown, et al.
384 1998; Burt, et al. 1998). In this sense, our results show that – at least in some cases – the
385 rhyolite-MELTS geobarometer can be used to constrain mineral assemblage, which is
386 particularly useful in the case of extraction pressures (see Gualda, et al. 2019b).

387 **Plagioclase, orthopyroxene, and magnetite geobarometry**

388 An alternative approach to solving the problem of the f_{O_2} sensitivity of plagioclase + pyroxene
389 geobarometry is to add a third phase to reduce the degrees of freedom. Although the PCC
390 magmas are quartz-absent, the erupted rocks all have magnetite phenocrysts (Table 1). In
391 Figure 7, we therefore plot the saturation surface of magnetite in addition to plagioclase and
392 orthopyroxene. As an Fe-bearing phase, magnetite is also sensitive to f_{O_2} . The saturation
393 temperature of magnetite increases as f_{O_2} increases, the inverse relationship to
394 orthopyroxene. This inverse relationship is expected, given that orthopyroxene predominantly
395 incorporates Fe^{2+} into its mineral structure whereas magnetite incorporates Fe^{3+} . This means
396 that it is possible to find a three-phase intersection of plagioclase + orthopyroxene +
397 magnetite by incrementally adjusting f_{O_2} . Magnetite is much more sensitive to f_{O_2} than
398 orthopyroxene, so smaller f_{O_2} steps are necessary. From visual inspection of the example in
399 Figure 7, the three-phase intersection must occur between NNO -1 and NNO -0.5. We
400 therefore perform a binary search, first performing geobarometry calculations in 0.25 log
401 intervals followed by 0.125 log intervals. We note, however, that rhyolite-MELTS is not precise
402 to three decimal places so the significance of the second and third decimal places should not
403 be overinterpreted. By performing this binary search, we find a three-phase intersection at
404 NNO -0.75 for the composition shown in Figure 7.

405 To test this procedure, we search for plagioclase + orthopyroxene + magnetite intersections
406 on every PCC composition. By visual inspection of the phase diagrams, we determine that the
407 three-phase intersection must occur between NNO -1.25 and NNO for every composition
408 (e.g., Figure 7). We therefore repeat the geobarometry calculations for each PCC composition
409 at nine intervals between NNO -1.25 and NNO (i.e., 0.125 log steps), keeping all other model
410 parameters the same (see Methods). Although inspection of the phase diagrams reveal three-
411 phase intersections for most compositions (Figure 7), only 4 of the 33 compositions return a

412 result using the parabola-fitting procedure shown in Figure 2. We therefore follow the
413 methodology of Harmon, et al. (2018) and increase the residual temperature threshold to 10
414 °C. Because the magnetite saturation temperature is so sensitive to f_{O_2} , a larger threshold is
415 reasonable to avoid false negatives. With a 10 °C threshold, 24 of the 33 compositions return
416 a result. Geobarometry results using a 5 °C, 8 °C, and 10 °C threshold are included in Online
417 Resource 4. The overall pressure distribution is unchanged.

418 The plagioclase + orthopyroxene + magnetite pressures for the PCC samples are between 39
419 and 142 MPa, in excellent agreement with independent pressure estimates for PCC (Table 2).
420 This suggests that the addition of magnetite improves the performance of the plagioclase +
421 orthopyroxene geobarometer in quartz-absent magma and is an elegant solution to
422 simultaneously constrain pressure and f_{O_2} .

423 In addition, the f_{O_2} at which these intersections occur (NNO -0.5 to NNO -1.125) overlaps with
424 f_{O_2} estimated for the PCC magma using Fe-Ti oxides with the Ghiorso and Evans (2008)
425 oxythermobarometer (NNO -0.1 to NNO -0.9, Figure 8). The Fe-Ti oxides suggest that the
426 1921-1922 had the most oxidising f_{O_2} , 1960 was slightly more reducing, and 2011-2012 was
427 much more reducing (Table 2). This trend is also apparent in the f_{O_2} estimated with the
428 plagioclase + orthopyroxene + magnetite geobarometer (Figure 8). This agreement is excellent
429 given the errors associated with each method.

430 Implications

431 Quartz + plagioclase geobarometry as maximum pressure estimates

432 The most important implication of the relationships between quartz, feldspar, and
433 orthopyroxene demonstrated in Figure 5 is that the maximum possible equilibration pressure
434 of a rhyolite is given by the quartz + feldspar intersection, regardless of whether quartz is
435 present in the system (Pamukçu, et al. 2021). The quartz + feldspar pressure results from
436 rhyolite-MELTS have been repeatedly shown to compare well to other geobarometers (Al-in-
437 hornblende and H₂O-CO₂ volatile saturation; Bégué, et al. 2014b; Gualda, et al. 2019a;
438 Pamukçu, et al. 2015). The quartz + feldspar pressures are relatively insensitive to fluid
439 saturation (Ghiorso and Gualda 2015; Gualda and Ghiorso 2014), and, as shown in Figure 5,
440 are insensitive to f_{O_2} . Uncertainty on the quartz + feldspar geobarometer due to analytical

441 uncertainty are on the order of 10-40 MPa 1σ , which depend on uncertainties associated with
442 the used compositions (Gualda and Ghiorso 2014; Gualda, et al. in review; Pamukçu, et al.
443 2021; Pitcher, et al. 2021; Smithies, et al. 2024; Smithies, et al. 2023). The quartz + feldspar
444 geobarometer therefore provides a useful constraint on the equilibration pressure of
445 rhyolites, even in cases in which they are not quartz-saturated (see also Blundy and Cashman
446 2001; Gualda and Ghiorso 2013b).

447 **Estimating f_{O_2}**

448 A persistent challenge to plagioclase + pyroxene geobarometry is the sensitivity of the
449 pressure results to f_{O_2} (Harmon, et al. 2018). We show that this uncertainty can be reduced
450 with two methods: 1) using independent estimates of f_{O_2} (e.g., Fe-Ti oxides) (Figure 6); and 2)
451 searching in f_{O_2} space for plagioclase + orthopyroxene + magnetite intersections (Figure 8). By
452 adding magnetite, we can obtain more precise pressure estimates for quartz-absent systems,
453 including systems where we have little independent information about f_{O_2} . The success of the
454 plagioclase + orthopyroxene + magnetite pressures is particularly important given that the
455 pyroxene geobarometry results are sensitive to volatile concentrations, especially in volatile-
456 undersaturated intermediate magma (Harmon, et al. 2018), and the pyroxene model in
457 rhyolite-MELTS may not correctly predict the stability of clinopyroxene (see Brugman and Till
458 2019; Wieser, et al. 2025). The results shown in Figure 8 also demonstrate that it is possible
459 to use the geobarometry procedure to obtain an estimate of f_{O_2} from melt composition alone.

460 **Beyond two- or three-phase rhyolite-MELTS geobarometers**

461 In previous parts of this series (Bégué, et al. 2014b; Gualda and Ghiorso 2014; Harmon, et al.
462 2018; Pamukçu, et al. 2015) the quartz + feldspar, quartz + 2 feldspar, plagioclase + pyroxene,
463 and the plagioclase + 2 pyroxene geobarometers were treated as separate entities. The
464 methods that we have shown here, and the examples in Figures 2, 5, and 7, show how rhyolite-
465 MELTS can be applied to search for the equilibration pressure between melt and any mineral
466 assemblage of interest, within the constraints of the existing MELTS models.

467 Rhyolite-MELTS geobarometry does not need to be limited to just two or three mineral phases
468 (Foley, et al. 2020; Gualda, et al. in review). For example, Figure 9 shows a four-phase
469 assemblage of quartz + plagioclase + orthopyroxene + magnetite for an extraction pressure

470 calculation for a whole-rock composition from the TVZ. As with the three-phase plagioclase +
471 orthopyroxene + magnetite calculations, we search in f_{O_2} space for the intersections of
472 multiple phases. Although the example in Figure 9 does not give any further pressure
473 information than a two-phase assemblage, the multiple phase assemblage reduces the
474 degrees of freedom in compositional space and gives more confidence to the pressure
475 calculation. If all we are interested in is pressure, searching in f_{O_2} space for an orthopyroxene
476 + quartz + plagioclase solution does not provide further pressure information.
477 Consequentially, the quartz + feldspar geobarometer of Gualda and Ghiorso (2014) is useful
478 for magma saturated in quartz and feldspar, without the need to add other phases (c.f.
479 multiply saturated geobarometers, Blundy 2022). However, a multiple-phase solution has
480 fewer degrees of freedom than a two-phase solution, so three- or four- phase pressure results
481 will have smaller uncertainties resulting from analytical error (Gualda and Ghiorso 2014;
482 Pamukçu, et al. 2021; Pitcher, et al. 2021; Smithies, et al. 2024; Smithies, et al. 2023).

483 Searching for relevant multiple phase intersections could be used to refine uncertain melt
484 compositions and intensive parameters. In the examples presented here, we have shown that
485 three-phase intersections that include Fe-bearing phases are useful for refining f_{O_2} . It would
486 also be informative to search within uncertainty of other parameters, for example adjusting
487 volatile content or major element compositions within analytical uncertainty. When the
488 composition is known, the coincidence of four or more phases increases our confidence that
489 – in some cases – the geobarometer can be used to infer likely mineral assemblages. The
490 Rhyolite-MELTS geobarometer is useful for more than just pressure when information from
491 multiple phases is investigated.

492 Conclusions

493 We demonstrate how rhyolite-MELTS can be used to search for equilibration pressures
494 between melt and any mineral assemblage of interest (within the limitations of rhyolite-
495 MELTS), and give examples of quartz, plagioclase, orthopyroxene, and magnetite. The rhyolite-
496 MELTS geobarometry results must be interpreted carefully as only mineral assemblages on
497 the simulated liquidus can be in equilibrium with the melt composition input by the user. We
498 hope this paper can be a guide to interpretation of rhyolite-MELTS results that move beyond
499 the established geobarometry applications.

500 If quartz is in equilibrium with the melt, then the two-phase quartz + feldspar geobarometer
501 is sufficient to estimate pressure; multiple saturation of additional phases does not further
502 constraint the pressure. In quartz-undersaturated magma, a useful relationship in rhyodacites
503 and rhyolites is that quartz + feldspar equilibration pressures are always maxima. At pressures
504 higher than the quartz + feldspar equilibration pressure, feldspar is undersaturated, which is
505 generally untenable for igneous rocks (e.g. Blundy and Cashman 2001; Gualda and Ghiorso
506 2013b). This means that even where quartz is not present, or in circumstances where we are
507 uncertain if quartz is saturated (e.g., when modelling melt extraction from an assumed mush
508 mineral assemblage), the rhyolite-MELTS quartz + feldspar geobarometer can still be used to
509 calculate maximum pressures.

510 In quartz-undersaturated magma, plagioclase + orthopyroxene \pm magnetite geobarometry
511 gives a useful estimate of pressure, despite the sensitivity of orthopyroxene and magnetite to
512 f_{O_2} . For PCC, plagioclase + orthopyroxene pressures calculated at independently determined
513 f_{O_2} are similar to independent pressure estimates. Alternatively, we can search within f_{O_2} space
514 to find the f_{O_2} at which plagioclase + orthopyroxene + magnetite saturate together. The f_{O_2}
515 and pressures estimated with this method for PCC are in excellent agreement with
516 independent estimates. This suggests there is potential to use rhyolite-MELTS geobarometry
517 not only to estimate pressure, but also to refine intensive parameters such as f_{O_2} by searching
518 in compositional space for multiple (≥ 3) mineral phase intersections.

519 Rhyolite-MELTS geobarometry does not need to be limited to three phases, and multiple
520 saturation of a higher number of phases can (1) give further constraints on intensive
521 parameters; (2) yield pressure estimates with smaller uncertainties; and (3) help determine
522 mineral assemblages that equilibrated with a given melt composition.

523 Authorship contribution statement

524 All authors contributed to the study conception. S. Smithies performed the data analysis,
525 wrote the first draft of the manuscript, and drafted the figures. All authors commented on and
526 revised subsequent versions of the manuscript.

527 Supplementary information

528 Online Resource 1: Spreadsheet of compositions used in this study with geobarometry results.

529 Online Resource 2: Animated version of Figure 5 showing orthopyroxene saturation surface
530 temperature decreasing as f_{O_2} increases.

531 Online Resource 3: Animated version of Figure 7 showing magnetite saturation surface
532 temperature increasing as f_{O_2} increases.

533 Online Resource 4: Plagioclase + orthopyroxene + magnetite geobarometry results for PCC as
534 in Figure 8 calculated with a residual temperature threshold of ≤ 8 °C and ≤ 5 °C.

535 Tables

536 **Table 1** Characteristics of the eruptions included in this study.

Volcanic centre	Eruption	Eruption age	Volume (km ³)	Phenocryst assemblage	Crystal content	f_{O_2}
Taupō Volcanic Zone (TVZ), Aotearoa New Zealand	Mamaku	240 ± 11 ka ^a	100	Plagioclase > quartz > orthopyroxene + Fe-Ti oxides > ± tr. augite ± tr. hornblende ^d	5-7 vol.% ^d	QFM 0 to +0.8 ^j
	Ohakuri	240 ± 11 ka ^b	150	Plagioclase > quartz > orthopyroxene > Fe-Ti oxides ^e	<5 vol.% ^e	QFM 0 to +0.8 ^j
	Pokai	275 ± 20 ka ^a	100	Plagioclase > orthopyroxene > quartz > Fe-Ti oxides > ± tr. clinopyroxene ± tr. amphibole ^f	2-8 vol.% ^f	QFM -0.2 to +0.6 ^{k,l}
	Kaingaroa	298 ± 3 ka ^c	100	Plagioclase > orthopyroxene > Fe-Ti oxides > ± tr. hornblende ± tr. augite ± tr. quartz ^g	<3.5 wt.% ^g	QFM 0 to +0.4 ^m
	Chimp	ca. 310 ka	50	Plagioclase > orthopyroxene + Fe-Ti oxides > > ± amphibole ± tr. clinopyroxene ± tr. quartz ± tr. biotite	<8 vol.% ^f	QFM +0.3 ^l
Puyehue-Cordón Caulle (PCC), Chile	1921-1922 (CCV)	1921-1922 CE	0.4	Plagioclase + orthopyroxene + clinopyroxene + spinel ^h	5-15% ^h	NNO -0.4 to -0.1 ^{n,o}
	1960 (CCVI)	1960 CE	0.25	Plagioclase + orthopyroxene + clinopyroxene + spinel ^h	5-15% ^h	NNO -0.5 to -0.2 ^{n,o}
	2011-2012	2011-2012 CE	1.5	plagioclase > orthopyroxene > clinopyroxene > magnetite + ilmenite ⁱ	5 vol.% ⁱ	NNO -0.9 to -0.8 ^{o,p,q}

537

538 Age references: a) Leonard (2003); b) Gravley, et al. (2007); c) Downs, et al. (2014).

539 Petrography references: d) Milner, et al. (2003); e) Gravley (2004); f) Karhunen (1993); g)

540 Beresford, et al. (2000); h) Gerlach, et al. (1988) i) Castro, et al. (2013).

541 f_{O_2} references, all calculated with the oxythermobarometer of Ghiorso and Evans (2008): j)
542 Bégué, et al. (2014a) k) recalculated from oxide compositions reported by Deering, et al.
543 (2010); l) recalculated from oxide compositions reported by Karhunen (1993); m) recalculated
544 from oxide compositions reported by Beresford, et al. (2000); n) Gerlach, et al. (1988); o)
545 Mingo (2019); p) Castro, et al. (2013); q) Jay, et al. (2014).

546

547

548 **Table 2** Comparison of pre-eruptive storage pressure estimates for the 2011 PCC eruption
 549 using independent petrologic and geophysical techniques.

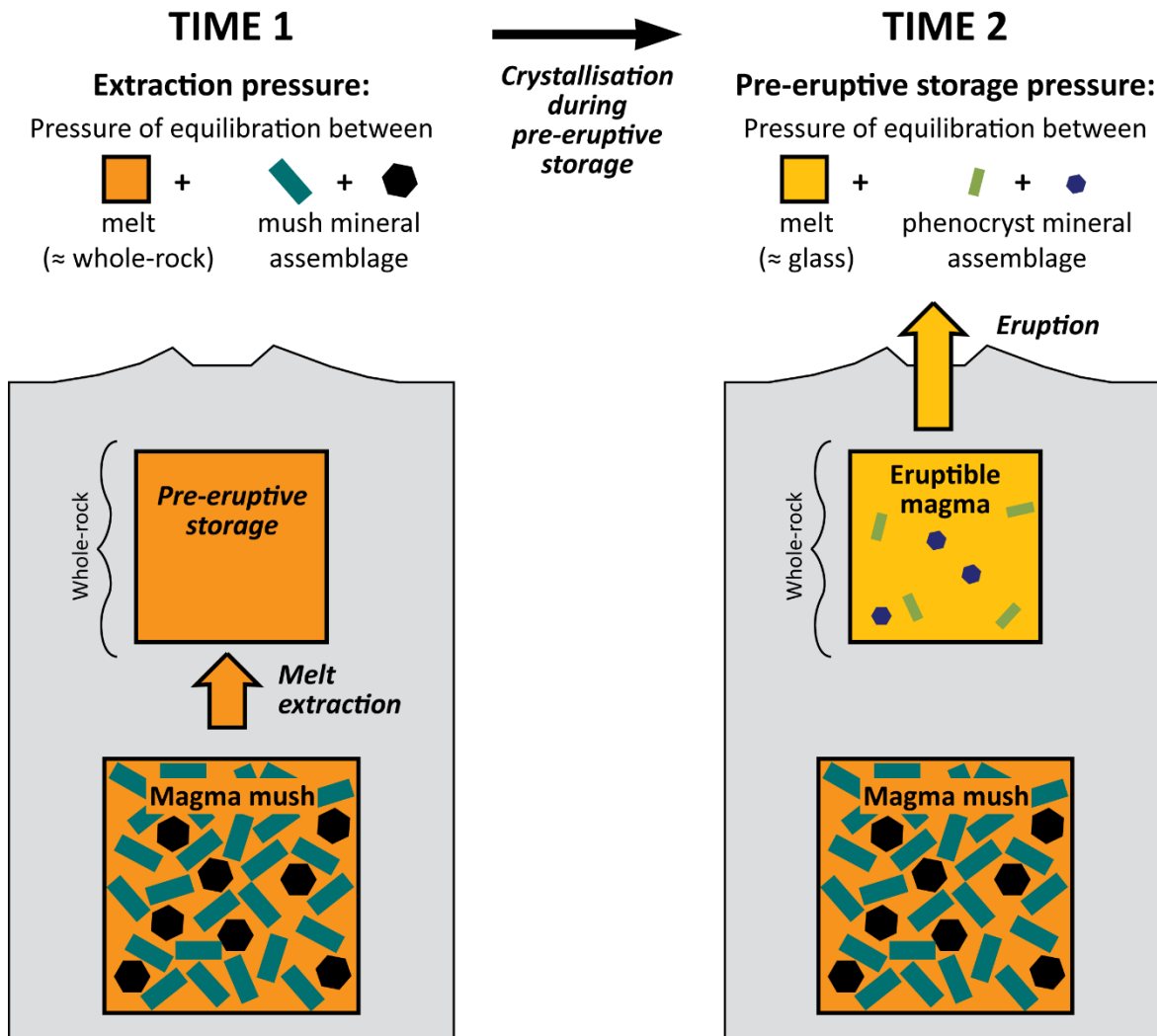
Pressure estimate method	H ₂ O-CO ₂ geobarometer*	Petrologic experiments	Inflation source modelled from InSAR [†]	Rhyolite-MELTS plagioclase + pyroxene geobarometer at ΔNNO -1.0	Rhyolite-MELTS plagioclase + pyroxene geobarometer at ΔNNO -0.75	Rhyolite-MELTS plagioclase + pyroxene + magnetite geobarometer
	Jay, et al. (2014)	Castro, et al. (2013)	Delgado, et al. (2019); Jay, et al. (2014); Wendt, et al. (2017)	Seropian, et al. (2021); this study	Seropian, et al. (2021); this study	This study
P _{min}		50	90	25	49	39
P _{mean}	140			73	90	76
P _{max}		115	135	123	146	142

550 *In pyroxene glass inclusions (n=6) using the H₂O-CO₂ model of Papale, et al. (2006)

551 [†]Converted from depth assuming a crustal density of 2.3 g cm⁻³.

552 Figures

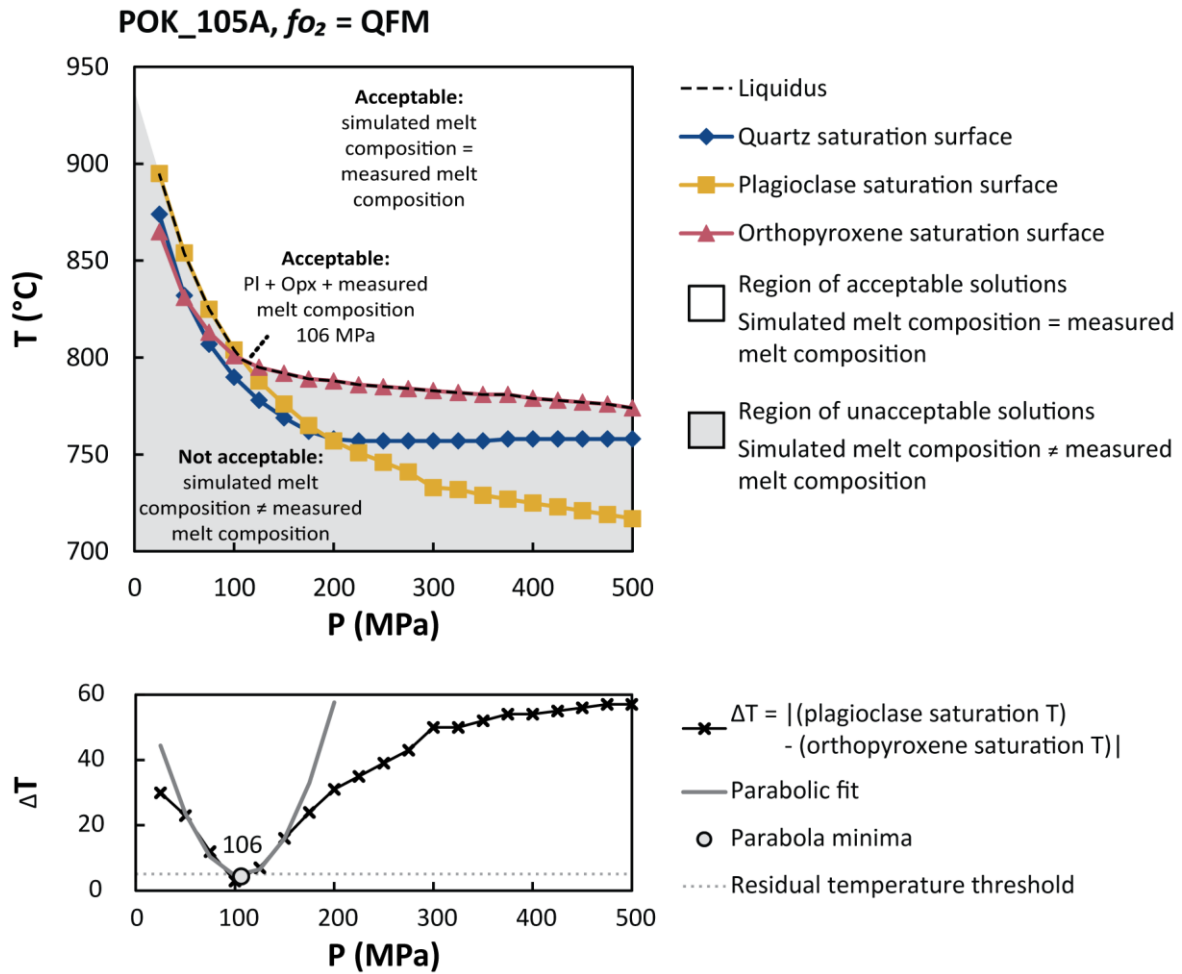
553



554

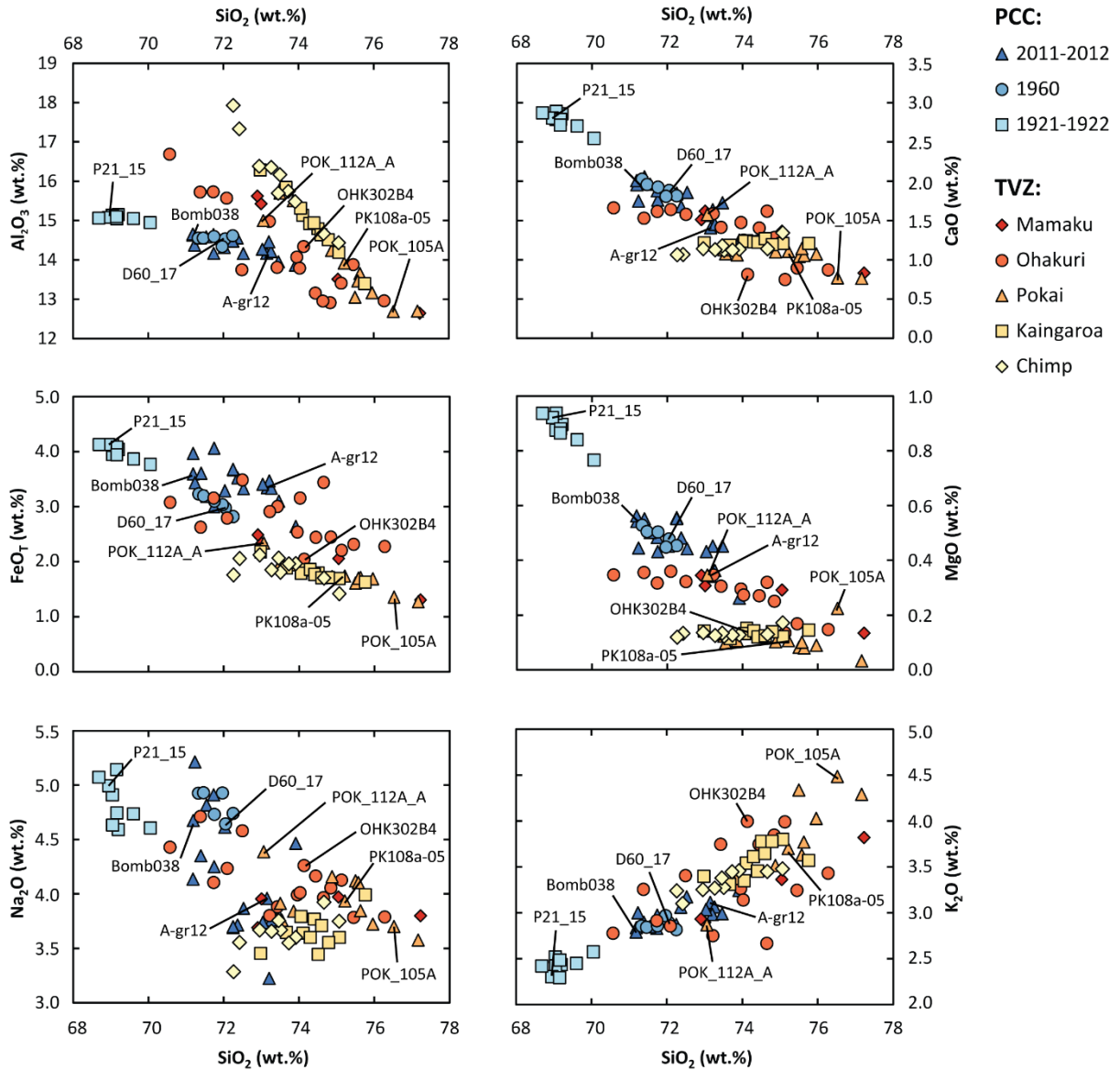
555 **Fig. 1** Conceptual magma system model after Gualda, et al. (2019b) showing definition of
556 extraction pressure (equilibration between bulk magma composition and the mush mineral
557 assemblage) and pre-eruptive storage pressure (equilibration between melt and crystals
558 immediately prior to eruption). In the case of extraction pressures, the mush mineral
559 assemblage is unknown, whilst in the case of storage pressures the phenocrysts could be
560 assumed to be in equilibrium with the glass composition.

561



562

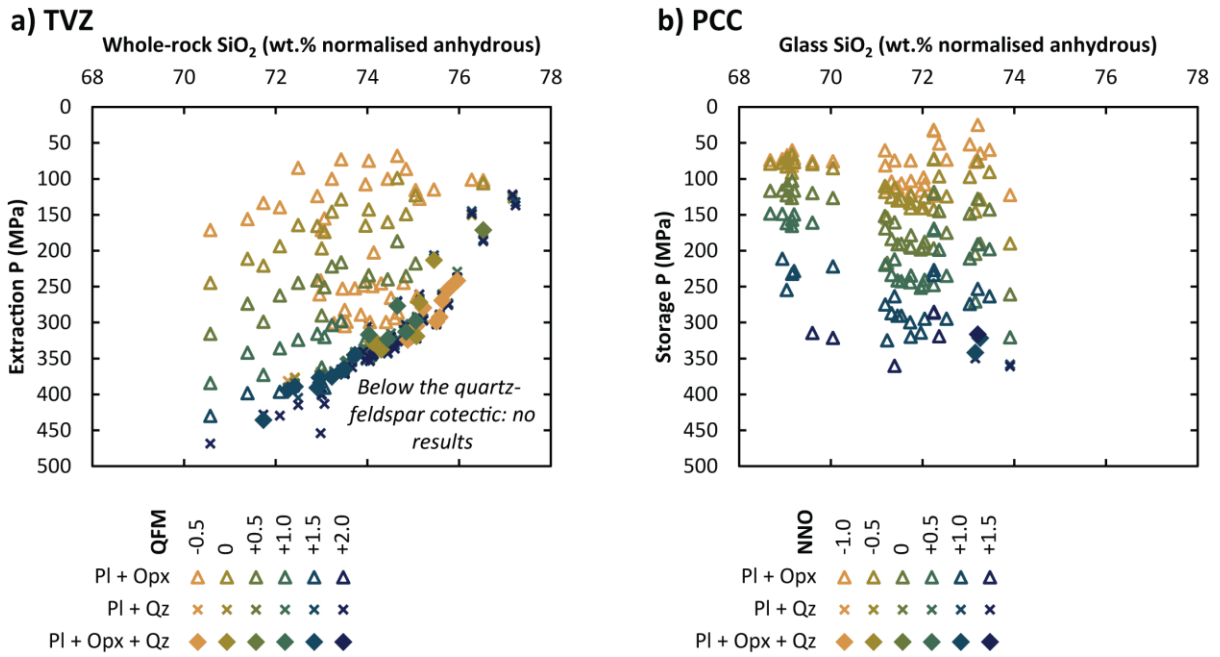
563 **Fig. 2** Top: pressure-temperature phase diagram result from a typical rhyolite-MELTS
 564 geobarometry calculation (sample POK_105A at the QFM buffer). Above the liquidus (dashed
 565 line) the melt composition simulated by rhyolite-MELTS is the same as the bulk composition
 566 of the system input by the user (i.e. the measured composition, a whole-rock pumice
 567 composition in this case). Below the liquidus the simulated melt is fractionated, so the
 568 simulated melt does not have the same composition as the measured melt composition. This
 569 means that pressure solutions for the measured melt composition must be on or above the
 570 liquidus. If both plagioclase and orthopyroxene are in equilibrium with the measured melt
 571 composition, the only possible pressure is at the intersection of the plagioclase and
 572 orthopyroxene saturation surfaces at 106 MPa. Bottom: illustration of parabola-fitting
 573 procedure to determine the pressure that the plagioclase and orthopyroxene saturation
 574 surfaces intersect. A parabola is fit along the lowest temperature difference and the
 575 temperature differences two pressure steps either side of the lowest temperature difference.
 576 The parabola-fitting procedure is only performed if $\Delta T \leq 5 \text{ } ^\circ\text{C}$ (the residual temperature
 577 threshold). This ensures that pressures are only calculated if there is a true intersection.



578

579 **Fig. 3** Major-element compositions from PCC (blue symbols) and TVZ (yellow-red symbols)
 580 samples used for the geobarometry calculations in this study. Compositions used as examples
 581 in Figures 2, 5, 6, 7, and 9 are labelled. All compositional data is included in Online Resource
 582 1.

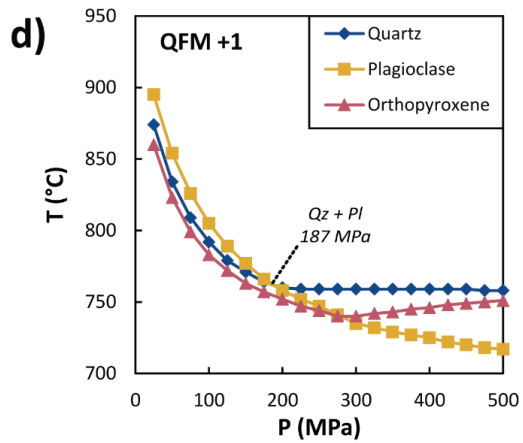
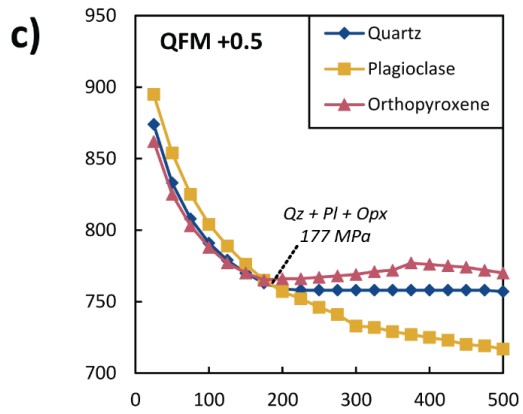
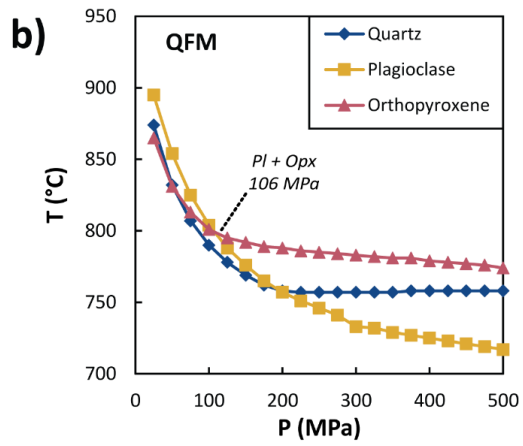
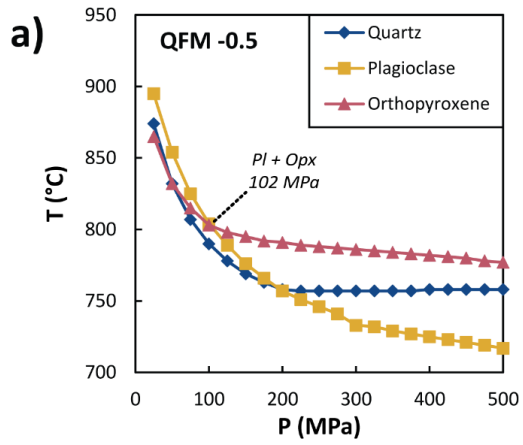
583



584

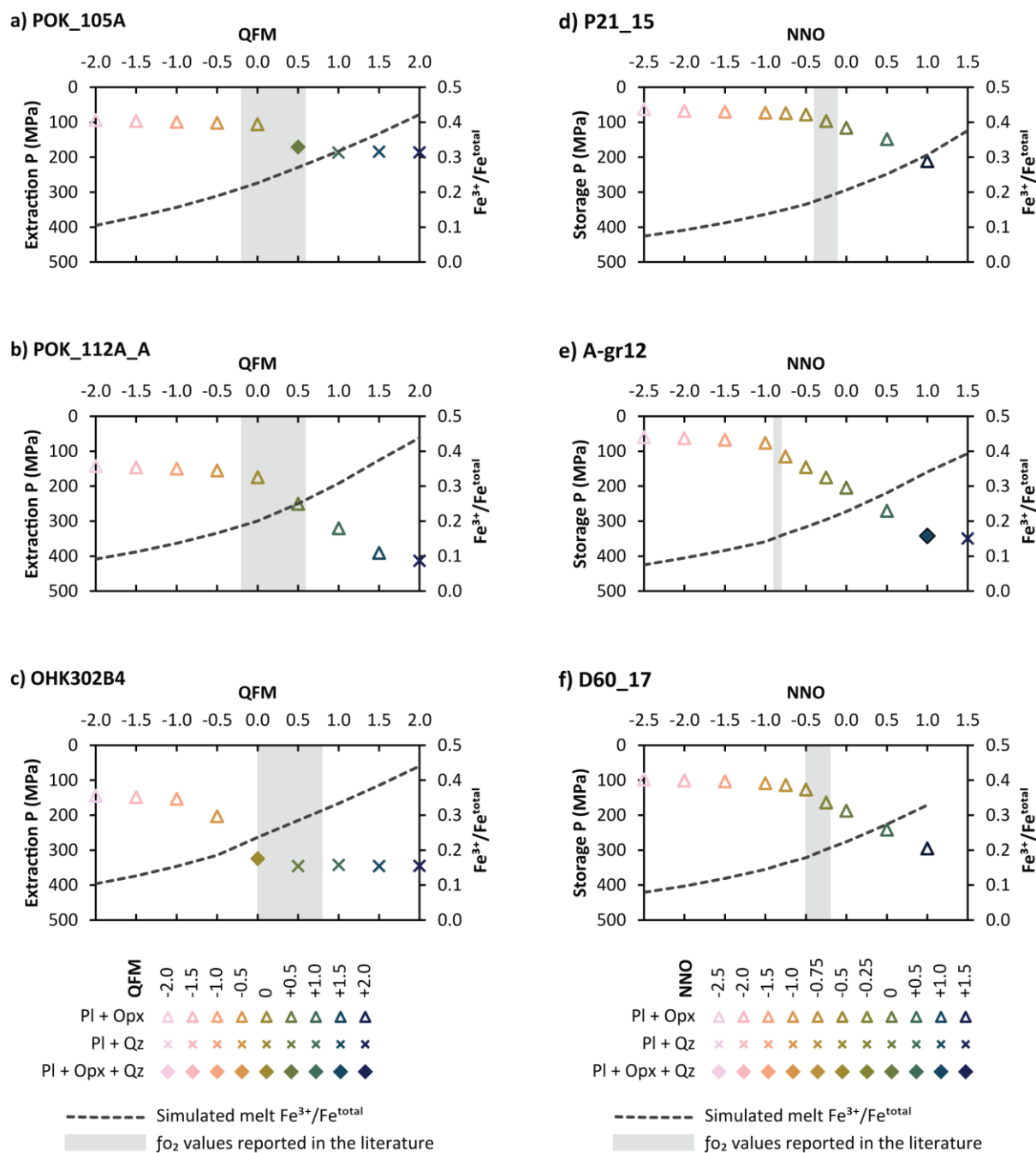
585 **Fig. 4** Geobarometry results for all compositions at various f_{O_2} (Online Resource 1). Symbol
 586 shape shows acceptable mineral assemblage as in Figure 6, symbol shading shows f_{O_2} as in
 587 Figure 6. In the high-silica rhyolites of the TVZ (a) there is a region below the quartz-feldspar
 588 cotectic where no pressure solutions are possible. This demonstrates that the quartz +
 589 feldspar geobarometer can be used to constrain maximum pressure.

590



592 **Fig. 5** Example of quartz + plagioclase + orthopyroxene saturation surfaces for the same model
593 inputs (sample POK_105A) but varying f_{O_2} . The quartz and plagioclase saturation
594 temperatures and pressures are invariable with f_{O_2} , whilst the orthopyroxene saturation
595 temperature decreases as f_{O_2} increases. At low f_{O_2} (QFM -0.5 and 0; a, b) the only acceptable
596 pressure results are plagioclase + orthopyroxene. At moderate f_{O_2} (QFM +0.5; c) there is a
597 three-phase plagioclase + orthopyroxene + quartz pressure solution. At high f_{O_2} (QFM +1; d)
598 orthopyroxene is no longer saturated on the liquidus so only quartz + plagioclase pressure
599 solutions are possible. An animated version of this figure showing an extended range of f_{O_2} is
600 available in Online Resource 2.

601

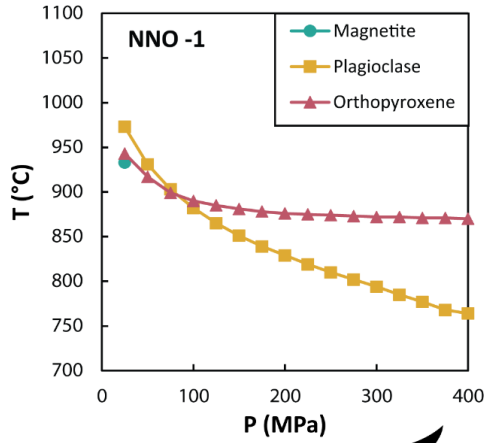


602

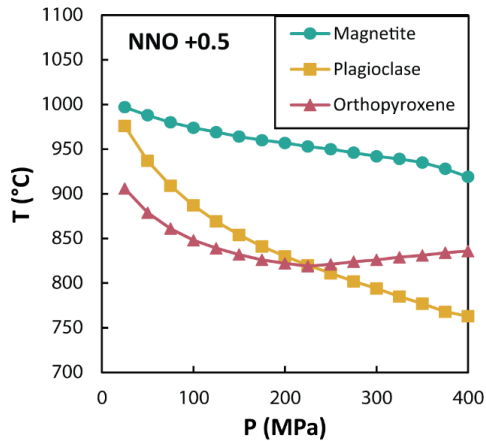
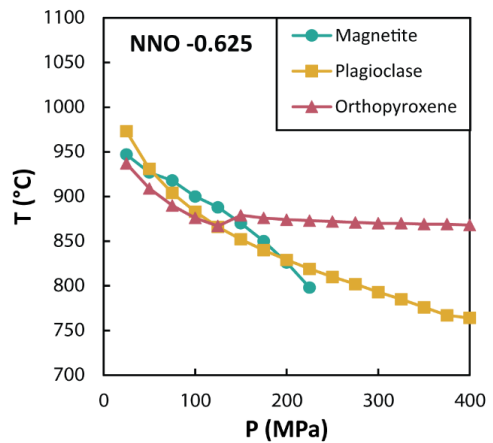
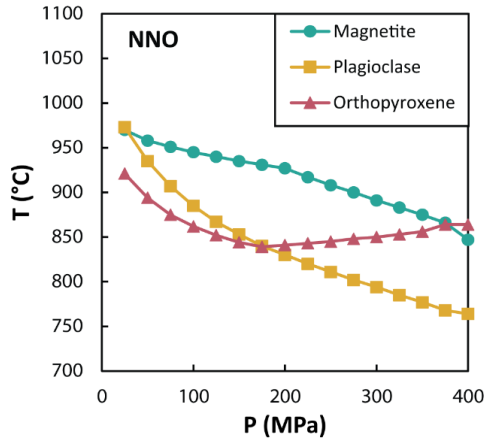
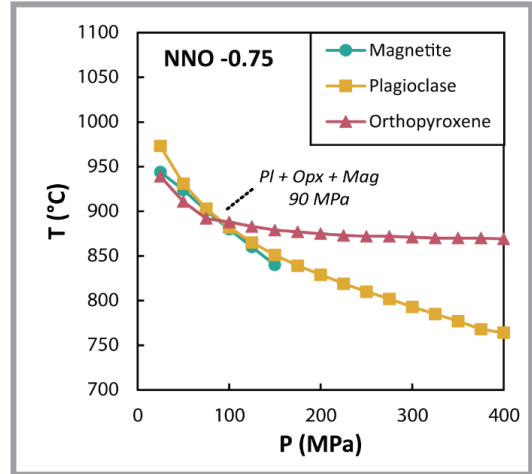
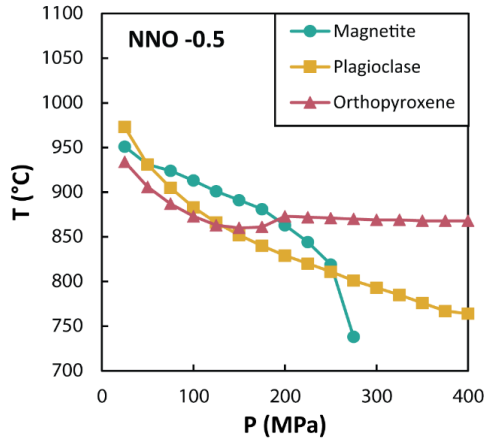
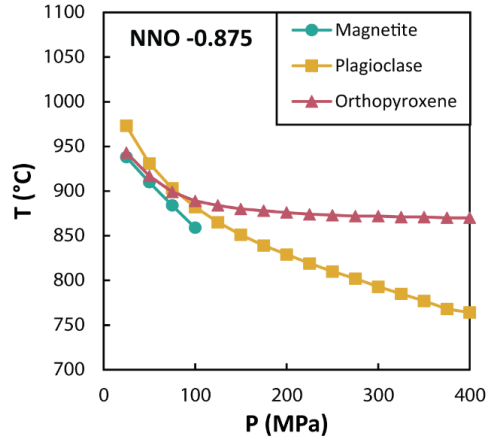
603 **Fig. 6** Three examples of geobarometry results from the TVZ (a-c) and PCC (d-f) as a function
 604 of f_{O_2} . Note that a) shows the same calculations as Figure 5. Symbol shape shows acceptable
 605 mineral assemblage as in Figure 4, symbol shading shows f_{O_2} as in Figure 4. Acceptable mineral
 606 assemblage shown with symbols. At low f_{O_2} the results are plagioclase + orthopyroxene
 607 (triangles), as f_{O_2} increases some compositions return quartz + plagioclase + orthopyroxene
 608 (diamonds), and at high f_{O_2} some compositions return quartz + plagioclase (crosses). The
 609 dashed line shows Fe^{3+}/Fe^{total} in the simulated liquid modelled by rhyolite-MELTS, this is

610 correlated with f_{O_2} leading to the sensitivity of pyroxene to f_{O_2} . The grey boxes show the range
611 of f_{O_2} reported for that eruption based on Fe-Ti oxides (see Table 1).

612

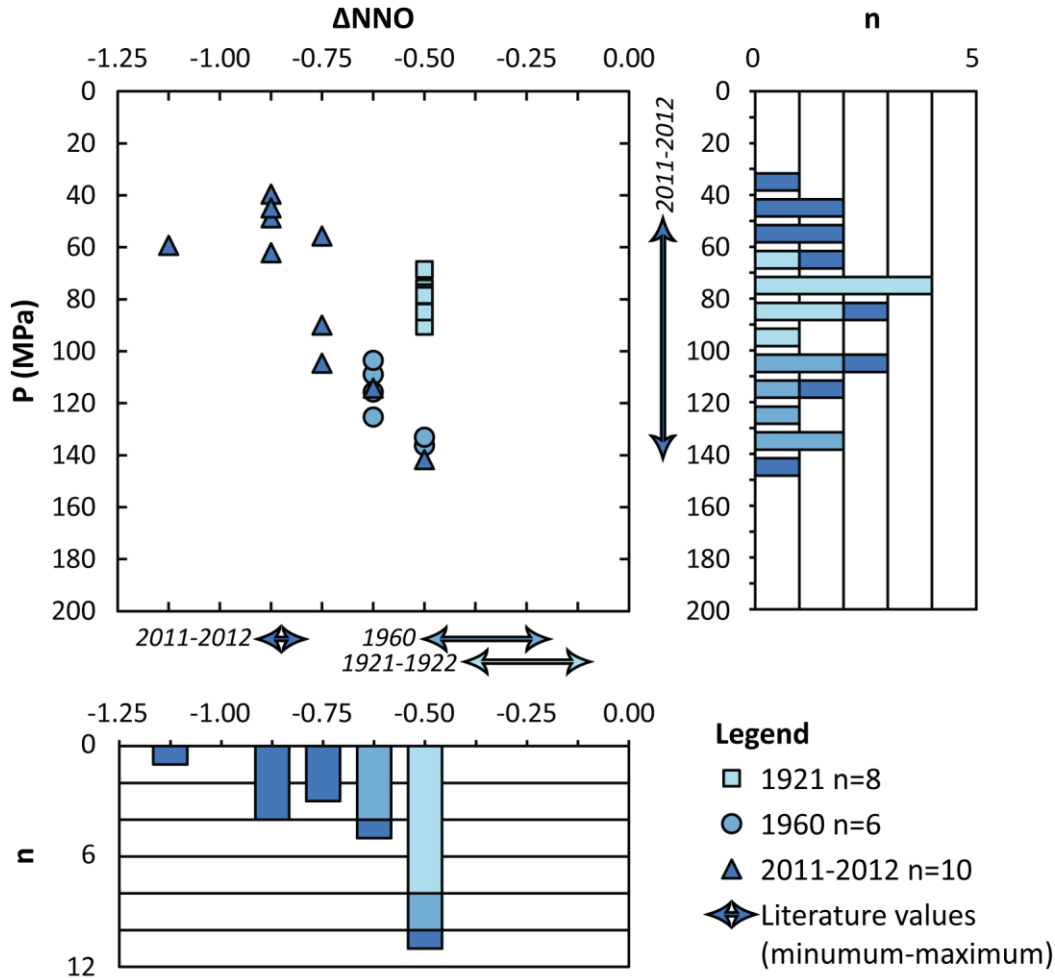


Smaller f_{O_2} increments to find plagioclase + orthopyroxene + magnetite solution



614 **Fig. 7** Example of plagioclase + orthopyroxene + magnetite saturation surface intersections at
615 varying f_{O_2} (sample Bomb038, PCC). The left column shows calculations performed at 0.5 log
616 interval f_{O_2} steps. The orthopyroxene saturation temperature moves down as f_{O_2} increases,
617 conversely, magnetite saturation temperature moves up as f_{O_2} increases. This means it is
618 possible to find a three-phase intersection by adjusting f_{O_2} . As magnetite is very sensitive to
619 f_{O_2} , small increments are necessary. In this example, the three-phase intersection must occur
620 between NNO -1 and NNO -0.5 (arrow). The right column therefore shows small 0.125 log
621 increment f_{O_2} steps between this interval. A three-phase solution is found at NNO -0.75, giving
622 a pressure of 90 MPa. An animated version of this figure showing saturation surfaces moving
623 with f_{O_2} is available in the Online Resource 3.

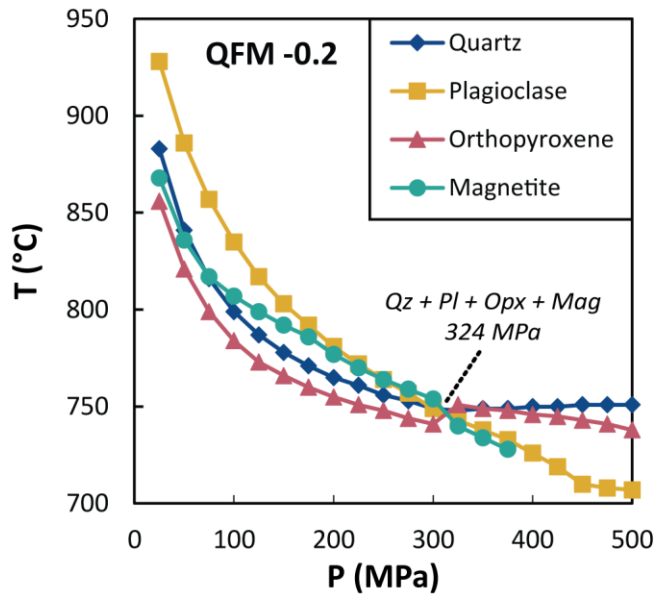
624



625

626 **Fig. 8** Plagioclase + orthopyroxene + magnetite geobarometry results for PCC compositions,
 627 showing both the pressure result and the f_{O_2} at which the three-phase intersection occurred.
 628 Results are calculated with a residual temperature threshold of ≤ 10 °C, see Online Resource 4
 629 for results with ≤ 8 °C and ≤ 5 °C thresholds. The arrows show the range of P and f_{O_2} for each
 630 eruption reported in the literature (see Table 2). There is excellent agreement between these
 631 independent P and f_{O_2} estimates and both the P and f_{O_2} results of the plagioclase +
 632 orthopyroxene + magnetite geobarometer.

633



634

635 **Fig. 9** Examples of a four-phase intersection (plagioclase + quartz + orthopyroxene +
636 magnetite) from sample PK108a-05 at QFM -0.2. This intersection does not provide any
637 further pressure constraint than a two- or three-phase intersection, but by reducing the
638 degrees of freedom we can constrain f_{O_2} (QFM -0.2) and the likely mineral assemblage (quartz-
639 bearing in this example).

640 References

- 641 Anderson Jr AT, Newman S, Williams SN, Druitt TH, Skirius C, Stolper E (1989) H₂O, CO₂, Cl, and gas in
642 Plinian and ash-flow Bishop rhyolite. *Geology* 17(3):221-225
- 643 Bachmann O, Dungan MA, Lipman PW (2002) The Fish Canyon Magma Body, San Juan Volcanic Field,
644 Colorado: Rejuvenation and Eruption of an Upper-Crustal Batholith. *J Petrol* 43(8):1469-1503
645 doi:10.1093/petrology/43.8.1469
- 646 Bégué F, Deering CD, Gravley DM, Kennedy BM, Chambefort I, Gualda GAR, Bachmann O (2014a)
647 Extraction, storage and eruption of multiple isolated magma batches in the paired Mamaku and
648 Ohakuri eruption, Taupo Volcanic Zone, New Zealand. *J Petrol* 55(8):1653-1684
649 doi:10.1093/petrology/egu038
- 650 Bégué F, Gualda GAR, Ghiorso MS, Pamukçu AS, Kennedy BM, Gravley DM, . . . Chambefort I (2014b)
651 Phase-equilibrium geobarometers for silicic rocks based on rhyolite-MELTS. Part 2: application to
652 Taupo Volcanic Zone rhyolites. *Contrib Mineral Petrol* 168(5):1-16 doi:10.1007/s00410-014-1082-7
- 653 Beresford SW, Cole JW, Weaver SD (2000) Weak chemical and mineralogical zonation in the Kaingaroa
654 Ignimbrite, Taupo volcanic zone, New Zealand. *New Zealand Journal of Geology and Geophysics*
655 43(4):639-650 doi:10.1080/00288306.2000.9514914
- 656 Black BA, Andrews BJ (2020) Petrologic imaging of the architecture of magma reservoirs feeding
657 caldera-forming eruptions. *Earth Planet Sci Lett* 552 doi:10.1016/j.epsl.2020.116572
- 658 Blundy J (2022) Chemical Differentiation by Mineralogical Buffering in Crustal Hot Zones. *J Petrol*
659 63(7):egac054
- 660 Blundy J, Cashman K (2001) Ascent-driven crystallisation of dacite magmas at Mount St Helens, 1980–
661 1986. *Contrib Mineral Petrol* 140(6):631-650
- 662 Brown SJA, Burt RM, Cole JW, Krippner SJP, Price RC, Cartwright I (1998) Plutonic lithics in ignimbrites
663 of Taupo Volcanic Zone, New Zealand; sources and conditions of crystallisation. *Chemical Geology*
664 148(1):21-41 doi:10.1016/S0009-2541(98)00026-6
- 665 Brugman KK, Till CB (2019) A low-aluminum clinopyroxene-liquid geothermometer for high-silica
666 magmatic systems. *American Mineralogist* 104(7):996-1004 doi:10.2138/am-2019-6842
- 667 Burgisser A, Scaillet B (2007) Redox evolution of a degassing magma rising to the surface. *Nature*
668 445(7124):194-197
- 669 Burnham CW (1994) Development of the Burnham model for prediction of H₂O solubility in magmas.
670 In: *Volatiles in magmas*, vol 30. De Gruyter, pp 123-130
- 671 Burt RM, Brown SJA, Cole JW, Shelley D, Waight TE (1998) Glass-bearing plutonic fragments from
672 ignimbrites of the Okataina caldera complex, Taupo Volcanic Zone, New Zealand: remnants of a
673 partially molten intrusion associated with preceding eruptions. *J Volcanol Geotherm Res* 84(3):209-
674 237 doi:10.1016/S0377-0273(98)00039-0
- 675 Caricchi L, Townsend M, Rivalta E, Namiki A (2021) The build-up and triggers of volcanic eruptions.
676 *Nature Reviews Earth & Environment*:1-19

- 677 Castro JM, Schipper CI, Mueller SP, Militzer AS, Amigo A, Parejas CS, Jacob DE (2013) Storage and
678 eruption of near-liquidus rhyolite magma at Cordon Caulle, Chile. *Bulletin of Volcanology* 75(4):1-17
679 doi:10.1007/s00445-013-0702-9
- 680 Cooper GF, Wilson CJN, Millet M-A, Baker JA, Smith EGC (2012) Systematic tapping of independent
681 magma chambers during the 1 Ma Kidnappers supereruption. *Earth Planet Sci Lett* 313:23-33
682 doi:10.1016/j.epsl.2011.11.006
- 683 Cottrell E, Birner SK, Brounce M, Davis FA, Waters LE, Kelley KA (2021) Oxygen fugacity across tectonic
684 settings. *Magma redox geochemistry*:33-61
- 685 Deering CD, Gravley DM, Vogel TA, Cole JW, Leonard GS (2010) Origins of cold-wet-oxidizing to hot-dry-
686 reducing rhyolite magma cycles and distribution in the Taupo Volcanic Zone, New Zealand. *Contrib*
687 *Mineral Petrol* 160(4):609-629 doi:10.1007/s00410-010-0496-0
- 688 Delgado F, Kubanek J, Anderson K, Lundgren P, Pritchard M (2019) Physicochemical models of effusive
689 rhyolitic eruptions constrained with InSAR and DEM data: A case study of the 2011-2012 Cordón Caulle
690 eruption. *Earth Planet Sci Lett* 524:115736
- 691 Downs DT, Rowland JV, Wilson CJN, Rosenberg MD, Leonard GS, Calvert AT (2014) Evolution of the
692 intra-arc Taupo-Reporoa basin within the Taupo volcanic zone of New Zealand. *10(1)*:185-206
693 doi:10.1130/GES00965.1
- 694 Edmonds M, Cashman KV, Holness M, Jackson M (2019) Architecture and dynamics of magma
695 reservoirs. *Philosophical Transactions of the Royal Society of London Series A: Mathematical, Physical,*
696 *and Engineering Sciences* 377(2139):20180298-20180298 doi:10.1098/rsta.2018.0298
- 697 Foley ML, Miller CF, Gualda GAR (2020) Architecture of a super-sized magma chamber and
698 remobilization of its basal cumulate (Peach Spring Tuff, USA). *J Petrol* 61(1)
699 doi:10.1093/petrology/egaa020
- 700 Gerlach DC, Frey FA, Moreno-Roa H, Lopez-Escobar L (1988) Recent volcanism in the Puyehue—Cordon
701 Caulle region, Southern Andes, Chile (40° 5° S): petrogenesis of evolved lavas. *J Petrol* 29(2):333-382
- 702 Ghiorso MS, Evans BW (2008) Thermodynamics of rhombohedral oxide solid solutions and a revision
703 of the Fe-Ti two-oxide geothermometer and oxygen-barometer. *American Journal of Science*
704 308(9):957-1039
- 705 Ghiorso MS, Gualda GAR (2013) A method for estimating the activity of titania in magmatic liquids
706 from the compositions of coexisting rhombohedral and cubic iron–titanium oxides. *Contrib Mineral*
707 *Petrol* 165(1):73-81 doi:10.1007/s00410-012-0792-y
- 708 Ghiorso MS, Gualda GAR (2015) An H₂O–CO₂ mixed fluid saturation model compatible with rhyolite-
709 MELTS. *Contrib Mineral Petrol* 169(6):1-30 doi:10.1007/s00410-015-1141-8
- 710 Giordano G, Caricchi L (2022) Determining the State of Activity of Transcrustal Magmatic Systems and
711 Their Volcanoes. *Annu Rev Earth Planet Sci Lett* 50(1):231-259 doi:10.1146/annurev-earth-032320-
712 084733
- 713 Gonnermann HM, Manga M (2007) The fluid mechanics inside a volcano. *Annu Rev Fluid Mech*
714 39(1):321-356

- 715 Graeter KA, Beane RJ, Deering CD, Gravley D, Bachmann O (2015) Formation of rhyolite at the Okataina
716 volcanic complex, New Zealand; new insights from analysis of quartz clusters in plutonic lithics. *Am*
717 *Mineral* 100(8-9):1778-1789 doi:10.2138/am-2015-5135
- 718 Gravley DM (2004) The Ohakuri pyroclastic deposits and the evolution of the Rotorua-Ohakuri
719 volcanotectonic depression. PhD. University of Canterbury
- 720 Gravley DM, Wilson CJN, Leonard GS, Cole JW (2007) Double trouble: Paired ignimbrite eruptions and
721 collateral subsidence in the Taupo Volcanic Zone, New Zealand. *Bulletin of the Geological Society of*
722 *America* 119(1-2):18-30 doi:10.1130/B25924.1
- 723 Gualda GAR, Bégué F, Pamukçu AS, Ghiorso MS (2019a) Rhyolite-MELTS vs DERP—Newer Does not
724 Make it Better: a Comment on ‘The Effect of Anorthite Content and Water on Quartz–Feldspar Cotectic
725 Compositions in the Rhyolitic System and Implications for Geobarometry’ by Wilke et al. (2017; *Journal*
726 *of Petrology*, 58, 789–818). *J Petrol* 60(4):855-864 doi:10.1093/petrology/egz003
- 727 Gualda GAR, Ghiorso MS (2013a) The Bishop Tuff giant magma body: an alternative to the Standard
728 Model. *Contrib Mineral Petrol* 166(3):755-775 doi:10.1007/s00410-013-0901-6
- 729 Gualda GAR, Ghiorso MS (2013b) Low-Pressure Origin of High-Silica Rhyolites and Granites. *The Journal*
730 *of Geology* 121(5):537-545 doi:10.1086/671395
- 731 Gualda GAR, Ghiorso MS (2014) Phase-equilibrium geobarometers for silicic rocks based on rhyolite-
732 MELTS. Part 1: Principles, procedures, and evaluation of the method. *Contrib Mineral Petrol* 168:1033
733 doi:10.1007/s00410-014-1033-3
- 734 Gualda GAR, Ghiorso MS (2015) MELTS_Excel: A Microsoft Excel-based MELTS interface for research
735 and teaching of magma properties and evolution. *Geochemistry, Geophysics, Geosystems* : G3
736 16(1):315-324 doi:10.1002/2014GC005545
- 737 Gualda GAR, Ghiorso MS, Hurst AA, Allen MC, Bradshaw RW (2022) A complex patchwork of magma
738 bodies that fed the Bishop Tuff supereruption (Long Valley 1 caldera, CA, USA): Evidence from matrix
739 glass major and trace-element compositions. *Frontiers in Earth Science*
740 doi:10.3389/feart.2022.798387
- 741 Gualda GAR, Gravley DM, Connor M, Hollmann B, Pamukçu AS, Bégué F, . . . Deering CD (2018) Climbing
742 the crustal ladder: Magma storage-depth evolution during a volcanic flare-up. *Science Advances*
743 4(10):eaap7567 doi:10.1126/sciadv.aap7567
- 744 Gualda GAR, Gravley DM, Deering CD, Ghiorso MS (2019b) Magma extraction pressures and the
745 architecture of volcanic plumbing systems. *Earth Planet Sci Lett* 522:118-124
746 doi:10.1016/j.epsl.2019.06.020
- 747 Gualda GAR, Miller CF, Wallrich BM (in review) The Rhyolite Factory: Insights from rhyolite-MELTS
748 geobarometry of plutonic rocks and associated volcanics. *J Petrol*
- 749 Hammarstrom JM, Zen Ea (1986) Aluminum in hornblende; an empirical igneous geobarometer. *Am*
750 *Mineral* 71(11-12):1297-1313
- 751 Harmon LJ, Cowlyn J, Gualda GAR, Ghiorso MS (2018) Phase-equilibrium geobarometers for silicic rocks
752 based on rhyolite-MELTS. Part 4: Plagioclase, orthopyroxene, clinopyroxene, glass geobarometer, and
753 application to Mt. Ruapehu, New Zealand. *Contrib Mineral Petrol* 173(1):1-20 doi:10.1007/s00410-
754 017-1428-z

- 755 Harmon LJ, Gualda GA, Gravley DM, Smithies SL, Deering CD (2024a) The Whakamaru magmatic
756 system (Taupō Volcanic Zone, New Zealand), part 1: Evidence from tephra deposits for the eruption of
757 multiple magma types through time. *J Volcanol Geotherm Res* 445:107966
- 758 Harmon LJ, Smithies SL, Gualda GA, Gravley DM (2024b) The Whakamaru Magmatic System (Taupō
759 Volcanic Zone, New Zealand), Part 2: Evidence from ignimbrite deposits for the pre-eruptive
760 distribution of melt-dominated magma and magma mushes. *J Volcanol Geotherm Res*:108013
- 761 Herzberg C (2004) Partial crystallization of mid-ocean ridge basalts in the crust and mantle. *J Petrol*
762 45(12):2389-2405
- 763 Holland T, Blundy J (1994) Non-ideal interactions in calcic amphiboles and their bearing on amphibole-
764 plagioclase thermometry. *Contrib Mineral Petrol* 116:433-447
- 765 Jay J, Costa F, Pritchard M, Lara L, Singer B, Herrin J (2014) Locating magma reservoirs using InSAR and
766 petrology before and during the 2011–2012 Cordón Caulle silicic eruption. *Earth Planet Sci Lett*
767 395:254-266
- 768 Jorgenson C, Higgins O, Petrelli M, Bégué F, Caricchi L (2022) A machine learning-based approach to
769 clinopyroxene thermobarometry: Model optimization and distribution for use in Earth sciences. *J*
770 *Geophys Res Solid Earth* 127(4):e2021JB022904
- 771 Karhunen RA (1993) The Pokai and Chimp ignimbrites of NW Taupo Volcanic Zone. PhD. University of
772 Canterbury
- 773 Lara L, Moreno H, Naranjo J, Matthews S, De Arce CP (2006) Magmatic evolution of the Puyehue–
774 Cordón Caulle Volcanic Complex (40 S), Southern Andean Volcanic Zone: from shield to unusual
775 rhyolitic fissure volcanism. *J Volcanol Geotherm Res* 157(4):343-366
- 776 Leonard GS (2003) The evolution of Maroa Volcanic Centre, Taupo Volcanic Zone, New Zealand. PhD.
777 University of Canterbury
- 778 Liu Y, Zhang Y, Behrens H (2005) Solubility of H₂O in rhyolitic melts at low pressures and a new empirical
779 model for mixed H₂O–CO₂ solubility in rhyolitic melts. *J Volcanol Geotherm Res* 143(1-3):219-235
- 780 Magee C, Stevenson CT, Ebmeier SK, Keir D, Hammond JO, Gottsmann JH, . . . Petronis MS (2018)
781 Magma plumbing systems: a geophysical perspective. *J Petrol* 59(6):1217-1251
- 782 Milner DM, Cole JW, Wood CP (2003) Mamaku Ignimbrite: a caldera-forming ignimbrite erupted from
783 a compositionally zoned magma chamber in Taupo Volcanic Zone, New Zealand. *J Volcanol Geotherm*
784 *Res* 122(3):243-264 doi:10.1016/S0377-0273(02)00504-8
- 785 Mingo MA (2019) Evaluation of Pre-eruptive Conditions for Cordon Caulle Rhyo-Dacitic Historic
786 Eruptions. Florida International University
- 787 Molina JF, Cambeses A, Moreno JA, Morales I, Montero P, Bea F (2021) A reassessment of the
788 amphibole-plagioclase NaSi-CaAl exchange thermometer with applications to igneous and high-grade
789 metamorphic rocks. *American Mineralogist* 106(5):782-800
- 790 Mutch E, Blundy J, Tattitch B, Cooper F, Brooker R (2016) An experimental study of amphibole stability
791 in low-pressure granitic magmas and a revised Al-in-hornblende geobarometer. *Contrib Mineral Petrol*
792 171:1-27

- 793 Newman S, Lowenstern JB (2002) VolatileCalc: a silicate melt–H₂O–CO₂ solution model written in
794 Visual Basic for Excel. *Computers & Geosciences* 28(5):597-604 doi:10.1016/S0098-3004(01)00081-4
- 795 Pamukçu AS, Gualda GAR, Ghiorso MS, Miller CF, McCracken RG (2015) Phase-equilibrium
796 geobarometers for silicic rocks based on rhyolite-MELTS—Part 3: Application to the Peach Spring Tuff
797 (Arizona–California–Nevada, USA). *Contrib Mineral Petrol* 169(3):549 doi:10.1007/s00410-015-1122-y
- 798 Pamukçu AS, Gualda GAR, Gravley DM (2021) Rhyolite-MELTS and the storage and extraction of large-
799 volume crystal-poor rhyolitic melts at the Taupō Volcanic Center: a reply to Wilson et al. (2021). *Contrib*
800 *Mineral Petrol* 176(10):82 doi:10.1007/s00410-021-01840-2
- 801 Pamukçu AS, Wright KA, Gualda GAR, Gravley D (2020) Magma residence and eruption at the Taupo
802 Volcanic Center (Taupo Volcanic Zone, New Zealand): insights from rhyolite-MELTS geobarometry,
803 diffusion chronometry, and crystal textures. *Contrib Mineral Petrol* 175(5) doi:10.1007/s00410-020-
804 01684-2
- 805 Papale P, Moretti R, Barbato D (2006) The compositional dependence of the saturation surface of H₂O+
806 CO₂ fluids in silicate melts. *Chemical Geology* 229(1-3):78-95
- 807 Pearce NJ, Westgate JA, Gualda GA, Gatti E, Muhammad RF (2020) Tephra glass chemistry provides
808 storage and discharge details of five magma reservoirs which fed the 75 ka Youngest Toba Tuff eruption,
809 northern Sumatra. *Journal of Quaternary Science* 35(1-2):256-271
- 810 Pistolesi M, Cioni R, Bonadonna C, Elissondo M, Baumann V, Bertagnini A, . . . Francalanci L (2015)
811 Complex dynamics of small-moderate volcanic events: the example of the 2011 rhyolitic Cordón Caulle
812 eruption, Chile. *Bulletin of Volcanology* 77:1-24
- 813 Pitcher BW, Gualda GA, Hasegawa T (2021) Repetitive duality of rhyolite compositions, timescales, and
814 storage and extraction conditions for pleistocene caldera-forming eruptions, Hokkaido, Japan. *J Petrol*
815 62(2):egaa106
- 816 Pritchard M, De Silva S, Michelfelder G, Zandt G, McNutt SR, Gottsmann J, . . . Finnegan N (2018)
817 Synthesis: PLUTONS: Investigating the relationship between pluton growth and volcanism in the
818 Central Andes. *Geosphere* 14(3):954-982
- 819 Putirka KD (2008) Thermometers and barometers for volcanic systems. *Reviews in Mineralogy and*
820 *Geochemistry* 69(1):61-120
- 821 Ridolfi F, Renzulli A, Puerini M (2010) Stability and chemical equilibrium of amphibole in calc-alkaline
822 magmas; an overview, new thermobarometric formulations and application to subduction-related
823 volcanoes. *Contrib Mineral Petrol* 160(1):45-66 doi:10.1007/s00410-009-0465-7
- 824 Schipper CI, Castro JM, Kennedy BM, Christenson BW, Aiuppa A, Alloway B, . . . Tuffen H (2019) Halogen
825 (Cl, F) release during explosive, effusive, and intrusive phases of the 2011 rhyolitic eruption at Cordón
826 Caulle volcano (Chile). *Volcanica* 2(1):73-90
- 827 Seropian G, Schipper CI, Harmon LJ, Smithies SL, Kennedy BM, Castro JM, . . . Forte P (2021) A century
828 of ongoing silicic volcanism at Cordon Caulle, Chile; new constraints on the magmatic system involved
829 in the 1921-1922, 1960 and 2011-2012 eruptions. *J Volcanol Geotherm Res* 420:107406
830 doi:10.1016/j.jvolgeores.2021.107406

- 831 Singer BS, Jicha BR, Harper MA, Naranjo JA, Lara LE, Moreno-Roa H (2008) Eruptive history,
832 geochronology, and magmatic evolution of the Puyehue-Cordón Caulle volcanic complex, Chile. *Geol*
833 *Soc Am Bull* 120(5-6):599-618
- 834 Smithies SL, Gravley DM, Gualda GA (2024) Connecting the Dots: the Lava Domes' Perspective of
835 Magmatism Related to an Ignimbrite Flare-Up. *J Petrol* 65(01):egad090
- 836 Smithies SL, Harmon LJ, Allen SM, Gravley DM, Gualda GAR (2023) Following magma: The pathway of
837 silicic magmas from extraction to storage during an ignimbrite flare-up, Taupō Volcanic Zone, New
838 Zealand. *Earth Planet Sci Lett* 607:118053 doi:10.1016/j.epsl.2023.118053
- 839 Tomiya A, Miyagi I, Saito G, Geshi N (2013) Short time scales of magma-mixing processes prior to the
840 2011 eruption of Shinmoedake volcano, Kirishima volcanic group, Japan. *Bulletin of Volcanology* 75:1-
841 19
- 842 Van Orman JA, Crispin KL (2010) Diffusion in oxides. *Reviews in Mineralogy and Geochemistry*
843 72(1):757-825
- 844 Voigt M, Coogan LA, von der Handt A (2017) Experimental investigation of the stability of clinopyroxene
845 in mid-ocean ridge basalts: the role of Cr and Ca/Al. *Lithos* 274:240-253
- 846 Wallace PJ, Anderson AT, Davis AM (1995) Quantification of pre-eruptive exsolved gas contents in silicic
847 magmas. *Nature* 377(6550):612-616
- 848 Weber G, Blundy J (2024) A machine learning-based thermobarometer for magmatic liquids. *J*
849 *Petrol*:egae020
- 850 Wendt A, Tassara A, Báez JC, Basualto D, Lara LE, García F (2017) Possible structural control on the
851 2011 eruption of Puyehue-Cordón Caulle Volcanic Complex (southern Chile) determined by InSAR, GPS
852 and seismicity. *Geophysical Journal International* 208(1):134-147
- 853 Wieser PE, Gleeson MLM, Matthews S, DeVitre C, Gazel E (2025) Determining the pressure-
854 temperature-composition (P-T-X) conditions of magma storage. In: Anbar A, Weis D (eds) *Treatise on*
855 *Geochemistry* (Third edition), vol 2. Elsevier, pp 83-151
- 856 Wieser PE, Kent AJ, Till CB, Abers GA (2023) Geophysical and geochemical constraints on magma
857 storage depths along the Cascade arc: Knowns and unknowns. *Geochemistry, Geophysics, Geosystems*
858 24(11):e2023GC011025
- 859 Wilke S, Holtz F, Neave DA, Almeev R (2017) The effect of anorthite content and water on quartz-
860 feldspar cotectic compositions in the rhyolitic system and implications for geobarometry. *J Petrol*
861 58(4):789-818 doi:10.1093/petrology/egx034
- 862 Winslow H, Ruprecht P, Gonnermann HM, Phelps PR, Muñoz-Saez C, Delgado F, . . . Amigo A (2022)
863 Insights for crystal mush storage utilizing mafic enclaves from the 2011-12 Cordón Caulle eruption.
864 *Scientific Reports* 12(1):9734-9734 doi:10.1038/s41598-022-13305-y
- 865 Yang H-J, Kinzler RJ, Grove TL (1996) Experiments and models of anhydrous, basaltic olivine-
866 plagioclase-augite saturated melts from 0.001 to 10 kbar. *Contrib Mineral Petrol* 124(1):1-18
- 867